Pergamon

Geochimica et Cosmochimica Acta, Vol. 68, No. 14, pp. 3019–3042, 2004

0016-7037/04 $30.00 + .00

doi:10.1016/j.gca.2004.02.009

Adsorption mechanisms of trivalent gold on iron- and aluminum-(oxy)hydroxides. Part 1: X-ray absorption and Raman scattering spectroscopic studies of Au(III) adsorbed on ferrihydrite, goethite, and boehmite

INGRID BERRODIER,[1,2] FRANÇOIS FARGES,[1,2,3,*] MARC BENEDETTI,[4] MARKUS WINTERER,[5] GORDON E. BROWN, JR.,[3,6] and MICHEL DEVEUGHÈLE[2]

[1]Laboratoire des géomatériaux, Université de Marne-la-Vallée FRE CNRS 2455, 77454 Marne la Vallée cedex 2, France
[2]Centre de Géologie de l'Ingénieur, ENSMP-ENPC-UMLV, FRE CNRS 2455 "G_2I," 77454 Marne la Vallée cedex 2, France
[3]Surface and Aqueous Geochemistry Group, Department of Geological and Environmental Sciences, Stanford University, Stanford, CA 94305-2115, USA
[4]UMR CNRS 7047, Université de Paris 6, 75251 Paris cedex 05, France
[5]Institut für Verbrennung und Gasdynamik, Universität Duisburg-Essen, Lotharstr. 1, 47057 Duisburg, Germany
[6]Stanford Synchrotron Radiation Laboratory, SLAC, 2575 Sand Hill Rd., MS 99, Menlo Park, CA 94025, USA

(*Received April* 28, 2003; *accepted in revised form February* 4, 2004)

Abstract—Gold adsorption products on powdered ferrihydrite, goethite, and boehmite samples, prepared by reacting Au(III)-Cl solutions ([Au] = 4.2×10^{-5}–9.0×10^{-3} M; [Cl] = 0.017–0.6 M) with these adsorbents at pH values of 4 to 9 and Au adsorption densities ranging from 0.046 to 1.53 μmol/m^2 were characterized using Au-L_{III} XAFS spectroscopy. The solutions (before and after uptake) were investigated by Raman scattering to determine speciation and by Inductively Coupled Plasma Atomic Emission Spectroscopy (ICP-AES) to determine solution composition. We present an analysis of several effects that are observed in the Au L_{III}-edge XAFS spectra, including X-ray beam-induced photo-reduction, multi-electronic excitations, disorder effects, and multiple scattering, that would complicate interpretation of the spectra if not accounted for. A combination of methods (spectral deconvolution, principal component analysis, spectral inversion, and wavelet analysis) was used to identify and quantify these effects, to characterize the nature of mixed ligands around gold, and to distinguish between multiple-scattering features and features due to next-nearest neighbors in the XAFS spectra.

Analysis of the Au-L_{III} XAFS spectra showed that Au(III) is present as square-planar Au(III)$(O,Cl)_4$ complexes in the aqueous solutions and on the surfaces of the Al/Fe-(oxy)hydroxide adsorption samples with dominantly O ligands at pH > 6 and mixed O/Cl ligands at lower pH values. The EXAFS-derived Au-O and Au-Cl distances are 2.00(2) and 2.28(2) Å, respectively, and the magnitudes of the Debye-Waller factors and third cumulants from anharmonic analyses indicate very little thermal or positional disorder around Au(III) in the adsorption samples. Iron second neighbors are present around Au in the Au(III)/ferrihydrite and Au(III)/goethite adsorption samples, with Au-Fe distances of 3.1(1) and 3.3(1) Å. In boehmite, two sets of Au-Al distances were detected at 3.0(1) and 3.2(1) Å. A reverse Monte Carlo study of the XAFS spectroscopic data suggests the presence of a continuum of edge-shared AuO_4-FeO_6 distances, which cannot be described correctly by a classical model of these data in which only a mean distance (although severely under-estimated) is derived.

1. INTRODUCTION

Gold is a strategic metal that can concentrate in iron-rich exogenetic horizons such as laterites (Brazil, Cameroon, Indonesia) or gossans (Canada, USA, France, among many others). Modeling the transport and deposition of gold under exogenetic conditions (see Seward, 1984, for a discussion of endogenetic hydrothermal transport of gold) requires an improved knowledge of the possible interactions between gold species in percolating aqueous solutions and mineral surfaces onto which gold can be adsorbed. The solubility of gold in these natural environments (see Schoonen et al., 1992) is controlled in part by adsorption reactions at mineral surfaces. For example, the concentration of gold in natural soils is usually very low (ppb level) when compared with predictions of gold dissolution using equilibrium thermodynamic calculations. The low gold concentration in soils suggests that the dissolution of gold is limited (see Benedetti and Boulegue, 1990) and/or that gold dissolution is inhibited by adsorption of gold onto minerals present in soils (Schoonen et al., 1992). Among the adsorption reactions of various moieties of gold available for transport (e.g., monovalent gold solution complexes, colloidal metallic gold, gold-sulfide/sulfite complexes interacting with organic matter, biogeochemical forms of gold in plants, etc.), the interactions of Au(III)-bearing solutions with fine-grained minerals such as iron- and aluminum-hydroxides are among the most important. These mineral phases are relatively abundant in many natural soils, and they have highly reactive surfaces (Sposito, 1984). Not surprisingly, gold anomalies (a few ppm) are commonly found in iron-rich soil profiles. The nature of this form of gold (so-called "invisible gold": see Gréffié et al., 1996) can be explained by the adsorption of gold during growth of the host mineral phase (Schoonen et al., 1992).

Ferrihydrites (or hydrous ferric oxides, HFOs) are poorly ordered iron hydroxides that are thought to play an important

* Author to whom correspondence should be addressed (farges@univ-mlv.fr).

role in the exogenetic geochemistry of trace elements because of their reactivity and large specific surface area (see Combes et al., 1989; Bottero et al., 1993; Drits et al., 1993; Manceau and Drits, 1993; Waychunas et al., 1996; Manceau and Gates, 1997; Brown et al., 1999). Iron- and aluminum-(oxy)hydroxides (including ferrihydrite, goethite (α-FeOOH), and boehmite (γ-AlOOH)) can sequester a wide range of transition elements, some of which are considered environmental pollutants. These finely divided phases can also sequester strategic and highly valuable elements such as gold (Schoonen et al., 1992; Gréffié et al., 1996; Karasyova et al., 1998). Some of the great occurrences of gold are associated with iron-(oxy)hydroxides in laterites or in gossans (see Machairas, 1963; Wilson, 1984; Mann, 1984; Michel, 1987; Zeegers, 1987; Butt, 1988; Benedetti and Boulegue, 1990; Grimm and Friedrich, 1990; Colin and Vieillard, 1991; Fressinet, 1991; Bowell et al., 1993a; Colin et al., 1989,1993; Sanfo et al., 1993). An improved knowledge of the adsorption mechanisms of Au on iron (oxy)hydroxides is, therefore, desirable to better understand the nature of "invisible gold," and how to optimize its extraction from such soils. This aspect is particularly important in developing countries where a number of micro-mining activities currently result in the misuse of harmful chemicals (e.g., mercury and cyanates) that have major impacts on the environment.

Previous studies of the adsorption of gold complexes on minerals (Jean and Bancroft, 1985; Fedoseyeva and Strel'tsova, 1987; Hyland and Bancroft, 1989; Mycroft et al., 1995; Widler and Seward, 2002) have shown that gold species present in solution can be reduced to metallic gold after exposure to oxidizable mineral surfaces (i.e., electron donating) such as metal sulfides. Gold can also be reduced and can precipitate by reacting with Fe^{2+}-bearing minerals or with Fe^{2+} released by the dissolution of such minerals (e.g., green rust-fougerite-related phases; see Mann, 1984; Webster and Mann, 1984) or, more importantly, with organic matter (such as fluvic and humic acids) present in soils (see Machesky et al., 1992; Bowell et al., 1993b; McInnes et al., 1996). The following reaction describes the reduction of Au(III) to Au(0) by Fe^{2+} in solution:

$$AuCl_4^- + 3Fe^{2+} + 6H_2O \Leftrightarrow Au^0 + 3FeOOH + 4Cl^- + 9H^+ \quad (1)$$

This reaction implies the simultaneous precipitation of gold and iron oxide. Bowell et al. (1993b) showed that, under acidic conditions, $AuCl_2^-$ and $AuOH(H_2O)^0$ aqueous complexes can be reduced by fluvic acid to form highly mobile bioinorganic gold colloids.

Adsorption of gold can also occur on redox-inactive materials such as alumina, kaolinite, hematite, and silica (see Nechayev, 1984; Nechayev and Nickolenko, 1986; Fedoseyeva and Zvonareva, 1988; Mitsyuk et al., 1991). Macroscopic studies of gold adsorbed on goethite and hematite surfaces (see Machesky et al., 1991; Karasyova et al., 1998) suggest that gold interacts with specific surface sites forming inner-sphere species such as $FeOHAuCl_3$ (for pH $\leq$ 4) or $Fe(OH)_2Au(OH)_2$ (at higher pH values). However, this type of studies (macroscopic uptake and modeling) cannot verify a particular sorption mode at the molecular scale. This can only be done using appropriate molecular-scale spectroscopic or scattering methods such as XAFS spectroscopy or surface-sensitive ^{197}Au Mossbauer spectroscopy. For example, the interaction of gold hydroxo-chloro complexes with Al/Fe-(oxy)hydroxides during coprecipitation experiments was investigated using ^{197}Au Mössbauer spectroscopy (Gréffié et al., 1996). However, because the redox state of gold was not assessed in a variety of Au-bearing iron-(oxy)hydroxides, the speciation of Au in these iron-(oxy)hydroxides and its mode of sorption to the mineral surfaces could not be derived using this method. On the other hand, Au-L_{III} edge X-ray absorption fine structure (XAFS) studies (including both the X-ray absorption near edge structure (XANES) and extended X-ray absorption fine structure (EXAFS) regions) are capable of identifying the speciation and the mode of sorption of many elements, including gold, to mineral surfaces (Brown, 1990; Farges et al., 1993; Berrodier et al., 1998,1999; Heasmann et al., 1998; Brown and Parks, 2001).

XAFS studies of Au at the L_{III} edge are complicated because of multi-electronic excitations and multiple-scattering events, as well as the possibility of X-ray beam-induced photo-reduction of Au, that makes analysis of the XAFS spectra challenging. Similarly, modeling absorption process (using CD-MUSIC methods, for instance; Hiemstra and van Riemsdijk, 1996; Hiemstra et al., 1989a,b) is also complicated and requires great care. Because of the variety of methods used in the present study, we have divided it into two parts. The first part includes a detailed description of the XAFS methods used to analyze gold L_{III} XANES and EXAFS spectra in this study, including an analysis of photo-reduction mechanisms, preedge features, multi-electron excitations, and multiple-scattering using various numerical tools such as principal component analysis (PCA), spectral deconvolutions, and wavelet analysis of the XAFS spectra. The first part also presents spectroscopic results (XAFS and Raman scattering) for trivalent gold speciation in solutions and on mineral surfaces.

2. EXPERIMENTAL

2.1. Starting Materials

Powdered goethite samples were prepared following the procedures of Johnson (1990) and Venema et al. (1996) under ambient conditions. Surface area determined using the Brunauer-Emmett-Teller (BET) method employing N_2 ranged from 78.8 to 79.2 m^2/g. Ferrihydrite (HFO) samples were also prepared at room temperature in polyethylene bottles, following two different protocols. One series of HFO samples was prepared by mixing 40 g of $Fe(NO_3)_3 \cdot 9H_2O$ in 0.5 L Milli-Q water and dropwise addition of 330 mL of 1 mol/L KOH. The KOH base was added to achieve a pH of 7–8. The solution was stirred vigorously during the titration, centrifuged, and washed repeatedly. A second set of HFO samples was prepared by dissolving 10 g of $FeCl_3$ in 250 mL Milli-Q water and adding KOH, until pH reached 7–8. Low BET surface area (3.2 m^2/g) boehmite samples used in this study were kindly provided by R. Gout via G. Morin (CNRS at the Laboratoire de Minéralogie-Cristallographie, Universities of Paris 6 and 7; see Castet et al., 1993, for details about these samples). In parallel, natural ferrihydrite (from a brook seeping over weathered basaltic lava of the Piton de la Fournaise volcano, Réunion Island, Indian Ocean) was used for other adsorption experiments.

Different gold stock solutions were prepared before the adsorption experiments (see Tables 1, 2, 3, and for details). In preparing the Au(III)/goethite adsorption samples, three stock solutions of the following compositions were used: (1) [Cl] = 0.1 mol/L and [Au] = 9×10^{-3} M, (2) [Cl] = 0.1 mol/L and [Au] = 9.5×10^{-4} M, and (3) [Cl] = 0.01 mol/L and [Au] = 3.45×10^{-3} M. For Au(III)/ferrihydrite adsorption samples prepared with ferrihydrites synthesized using reagent-grade iron(III) nitrate, three stock solutions of the following compositions were used: (1) [Cl] = 0.35 mol/L and [Au] = 3.0×10^{-3} M, (2) [Cl] = 0.02 mol/L and [Au] = 3.0×10^{-3} M, and (3) [Cl] = 0.6 mol/L and [Au] = 6.0×10^{-3} M. For Au(III)/ferrihydrite adsorption samples prepared with ferrihydrites synthesized using reagent-grade iron chloride, two stock solutions of the following compositions were used (1) [Cl] = 0.5 mol/L and [Au] = 3.8×10^{-3} M, and (2) [Cl] = 0.03 mol/L and [Au] = 3.8×10^{-3} M. For the Au(III)/boehmite adsorption samples, two stock solutions of the following compositions were used: (1) [Cl] = 0.1 mol/L and [Au] = 9.0×10^{-5} M, and (2) [Cl] = 0.01 mol/L and [Au] = 4.2×10^{-5} M. We also reexamined several of the solutions studied by Farges et al. (1993) and observed that after 10 yr of confinement in air/light-sealed containers, the speciation of gold remains unchanged. This finding suggests that the newer solutions prepared before the adsorption experiments presented in the current study are stable.

2.2. Adsorption Experiments

Various mixtures of gold-bearing solutions and Al/Fe-(oxy)-hydroxides were stirred overnight at a given synthesis pH (adjusted by 0.1 mol/L KOH and/or HNO3). Sorption kinetics reported by Machesky et al. (1991) and Gréffié et al. (1996) indicate that equilibrium should have been reached within 1 h before XAFS data collection, the solutions were centrifuged at 13,000 *g*. The gold concentration in solutions before adsorption experiments as well as in the supernatant solutions in contact with the equilibrated adsorbents were analyzed using ICP-AES (inductively coupled plasma atomic emission spectroscopy; detection limits 50 nmol L^{-1}; see Tables 1–4). The concentrations of adsorbed Au on the sorbents were obtained by difference between the Au solution concentrations before and after uptake and normalized to BET surface areas of 79 m^2/g and 3.2 m^2/g for goethite and boehmite, respectively. In the case of HFO, a value of 600 m^2/g was used as recommended by Davis (1977) and discussed by Dzomback and Morel (1990). The amount of adsorbed gold increases with increasing pH and decreasing ionic strength (details in Berrodier, 2001) as previously reported by Machesky et al. (1991) and Karasyova et al. (1998). No evidence for metallic gold formation was observed in the samples examined here (the presence of metallic gold is easily detectable by Au L_{III}-XANES spectra due to the much lower amplitude white line and energy-shifted edge position relative to Au(III)). Metallic gold was observed in several series of samples by XAFS spectroscopy; these samples were excluded from our study, the origin of that metallic "contamination" identified, the samples resynthesized and XAFS data recollected until a white line typical to Au(III) in position and intensity was obtained.

2.3. Sample Characterization

2.3.1. X-ray methods

Before spectroscopic investigation, all solid samples were characterized by X-ray diffraction methods and environmental scanning electron microscopy (ESEM) to check for sample homogeneity, crystallinity, and the presence of potential inclusions of metallic gold at the spatial scale of observation of these methods (dozens of μm to 0.01 μm). X-ray diffraction experiments were conducted on a Siemens 501 diffractometer (CGI facility, Ecole des Mines de Paris at Marne la Vallée), using Cu Kα radiation at 40 kV and 24 mA. Scans were collected over the 2θ range 2° to 62° (0.015° steps), using 1 s integration time per data point. For goethites and boehmites, the diffraction patterns are consistent with crystal structure refinements (Von Hoppe, 1941; Reichertz and Yost, 1946; Szytula et al., 1968; Gualtieri and Venturelli, 1999). The diffraction patterns for the freshly synthesized HFOs have two broad bands centered near 2.4 and 2.1 Å, which are related to O-O and Fe-O pair correlations, respectively (Drits et al., 1993).

2.3.2. Environmental scanning electron microscopy (ESEM)

ESEM images and semiquantitative elemental analyses were conducted on an Electroscan apparatus (E3 type; at the CESAM facility, Université de Marne la Vallée) under the following conditions: electron accelerating voltage of 30 keV, sample environment pressure of 0.01 atm, and detection using a secondary ion detection mode. Elemental analyses and imaging were performed by monitoring the intensity of the $L_{\alpha/\beta}$ X-ray emission spectra of gold, performed on a 1 μm^3 volume of sample. Systematic mapping of the Au-content for most samples showed that gold was homogeneously distributed. No metallic precipitate at the observation scale (0.5–50 μm) could be observed in most samples, which is in agreement with transmission electron microscopy (HRTEM) observations on Au coprecipitated on HFO (Gréffié et al., 1996). However, in some samples, precipitates of metallic gold were observed (related to sample synthesis problems). Therefore, these types of samples were excluded from further analyses.

2.4. Raman Scattering Spectroscopy

Unpolarized room temperature macro-Raman scattering spectra were recorded on gold-bearing solutions to determine qualitatively the gold speciation in solutions before and after uptake, to compare with structural information from XAFS spectroscopy, which averages the local environments for all Au-species. We used a DILOR™ XY double subtractive multichannel Raman spectrophotometer (ITODYS facility at the University of Paris 7) and collected the spectra between the 110–1100 cm-1 using a 1200 line/mm grating monochromator and an ORTEC CCD nitrogen-cooled detector. Raman modes were excited using the 514.5 nm line of an Ar+ laser. Typical recording conditions were 2–3 spectra with an incident laser power of 0.4 W. Spectral analyses were performed using the PeakFit package, by least-squares modeling of the experimental spectra using gaussian-shaped bands, for which positions were coarsely determined first from inspection of the second derivatives of the raw signal.

2.5. XAFS Spectroscopy

2.5.1. XAFS data collection

A first set of X-ray absorption fine structure (XAFS) spectra was collected at the Stanford Synchrotron Radiation Laboratory (SSRL, SPEAR2 storage ring, Stanford, USA), at the Au L_{III} edge (11,919 eV). Wiggler beam line 4–3 was used to collect these spectra with samples at ambient (290 K) and low temperatures (10 K, using a He-cooled cryostat). Either a Stern-Heald-Lytle detector or a 13-elements solid-state Canberra Ge detector was used to monitor the $L_{\alpha/\beta}$ fluorescence arising from gold. A second set of XAFS spectra was collected at 10 K on the EXAFS2 beamline at the Laboratoire pour l'Utilisation du Rayonnement Electromagnétique (DCI storage ring, LURE, Orsay, France) using a 7-element solid-state Canberra Ge detector. The SPEAR and DCI rings were operating at 3.0 and 1.8 GeV, respectively, with electron currents of 70–100 and 200–300 mA, respectively. The spectra were collected using Si(220) and Si(311) double crystal monochromators, respectively, at SSRL and LURE, detuned approximately 30% to reject high energy harmonics from the incident beam. The use of Si(111) monochromators would have resulted in more severe degradation of the sample (by photo-reduction, as explained below, because of their higher flux than Si(220) for the same spectrometer). Incident and transmitted X-ray fluxes were measured using ionization chambers filled with N_2. Fluorescence-yield spectra were measured using Ga and Ti filters to help remove, respectively, elastic scattering and Fe-K_α fluorescence (in Fe-bearing samples). Energy calibration was monitored using an Au foil (inflection point of the Au L_{III} edge was set at 11,919 eV) placed in front of the I_1 detector. Six to 15 scans were averaged for each sample to improve signal/noise ratio, and each spectrum was checked for photo-reduction effects (see below).

2.5.2. XAFS data analysis

XANES spectra were collected from 100 eV before to 250 eV after the Au-L_{III} edge, with 0.2 eV steps and 1 s/point integration time. Resolution analysis at both SSRL and LURE suggests that the Au-L_{III} edge core-hole lifetime ($\sim$ 4.5 eV: Krause and Oliver, 1979) is the main contributor to spectral broadening (experimental broadening is $\sim$ 1.2 eV on beam line 4–3 at SSRL, assuming also a 1 mm vertical slit opening before the monochromator and the sample hutch, respectively). EXAFS spectra were collected from 300 eV before to 1000 eV after the Au-L_{III} edge, with 2.5 eV steps (at LURE) or 0.04 $Å^{-1}$ steps (at SSRL), and integration times ranging from 1 s/point (just after the edge) to 5 s/point (at the end of each scan). To control photo-reduction events, a higher number of scans was collected per sample at a faster scanning speed rather than using integration times above 5 s per data point. Au-L_{III} edge XANES and EXAFS spectra were analyzed using the XAFS package of Winterer (1996). Spectra were normalized in absorbance using a Victoreen function (for the region before the Au-L_{III} edge) and a spline function (with 10 external double knots) for the postedge region. Energies were converted into *k*-space (*k* is the photoelectron momentum), with "E_0" (i.e., the energy where *k* is set to zero) arbitrarily chosen at the inflection point of an error function used to model the edge jump. To model first- or next-nearest neighbor contributions separately, the k^3-weighted spectra were Fourier transformed (FT) over the *k*-range of 3 to 15Å-1, using a Kaiser-Bessel function with a τ value of 4, and back-Fourier transformed (FT^{-1}) to extract the FT-filtered EXAFS signal corresponding to either the first- or next-nearest neighbors contributions. Both the normalized EXAFS and the FT-filtered EXAFS spectra were fitted using least-squares methods (Levenberg-Marquardt). Most fits were computed using normalized EXAFS spectra (least-squares fits of noisy spectra, especially those of Au/boehmites, were based on FT^{-1} spectra). An interpolation is required at some point in the XAFS background fitting and subtraction procedure, resulting in a slight smoothing of the high frequency noise, which has a slight effect on the normalized EXAFS spectra. For convenience, we will present the normalized EXAFS spectra before and after interpolation (the latter being used for fitting of the spectra of adsorption samples). We used the curve-wave EXAFS formalism (Rehr et al., 1986; Crozier et al., 1988) to derive the desired (average) structural information in k-space around the central gold atom, which includes identification of type of first- and next-nearest neighbor atoms, their number (N), their average distance to the central Au, a Debye-Waller type of factor (σ^2), and an anharmonic parameter (third cumulant or C_3). The σ^2 and C_3 parameters provide a measure of the relative disorder (harmonic and anharmonic, respectively) in the Au-O and Au-Cl pair correlations (relative to model compounds). In fitting the background-subtracted and normalized EXAFS of adsorption samples, backscattering phase-shift and amplitude functions for the O/Cl first neighbors were extracted from the EXAFS spectra of well-characterized crystalline model compounds, such as Au_2O_3 (Jones et al., 1979) and $KAuCl_4 \cdot 2H_2O$ (Theobald and Omrani, 1980). However, because of the lack of available model compounds, ab initio backscattering phase-shift and amplitude functions for Al/Fe second neighbors were calculated using FEFF 7 (Ankudinov et al., 1988; Rehr et al., 1992). For these FEFF calculations, we used the crystal structure of $LaAuO_3$ (Ralle and Jansen, 1993) that we modified by replacing La by Fe (or Al) and by adjusting the unit-cell parameters to obtain a local structure around Au consisting of corner-shared AuO_4 and Fe/AlO_6 polyhedra, with Au-Fe/Al distances of 3.0–3.3 Å (as is also observed in our Au-adsorption samples). Unfortunately, there are no AuFe-containing model compounds available to our knowledge (ICDS database), so we could not test the FEFF-calculated model. However, the FEFF XAFS spectra calculated for various model compounds of Au for which we have the experimental spectra (Au(I)I, Au(I)Cl, $Au(III)_2O_3$, $Au(III)(OH)_3$, $Au(III)Cl_3$, $KAuCl_4 \cdot 2H_2O$) resulted in excellent results (see later on Fig. 1c), suggesting that the XAFS spectrum calculated for the hypothetical $FeAuO_3$ structure is valid.

2.6. XAFS Spectral Artifacts

2.6.1. Identifying redox states of Au

As discussed previously (see Bassi et al., 1976; Lytle et al., 1979; Watkins et al., 1987), the Au-L_{III} edge position shifts dramatically with the redox state of gold (see Fig. 1a). Accordingly, the edge position for Au(I) is shifted to higher energy relative to that for metallic gold (by $\sim$ 2 eV). However, the

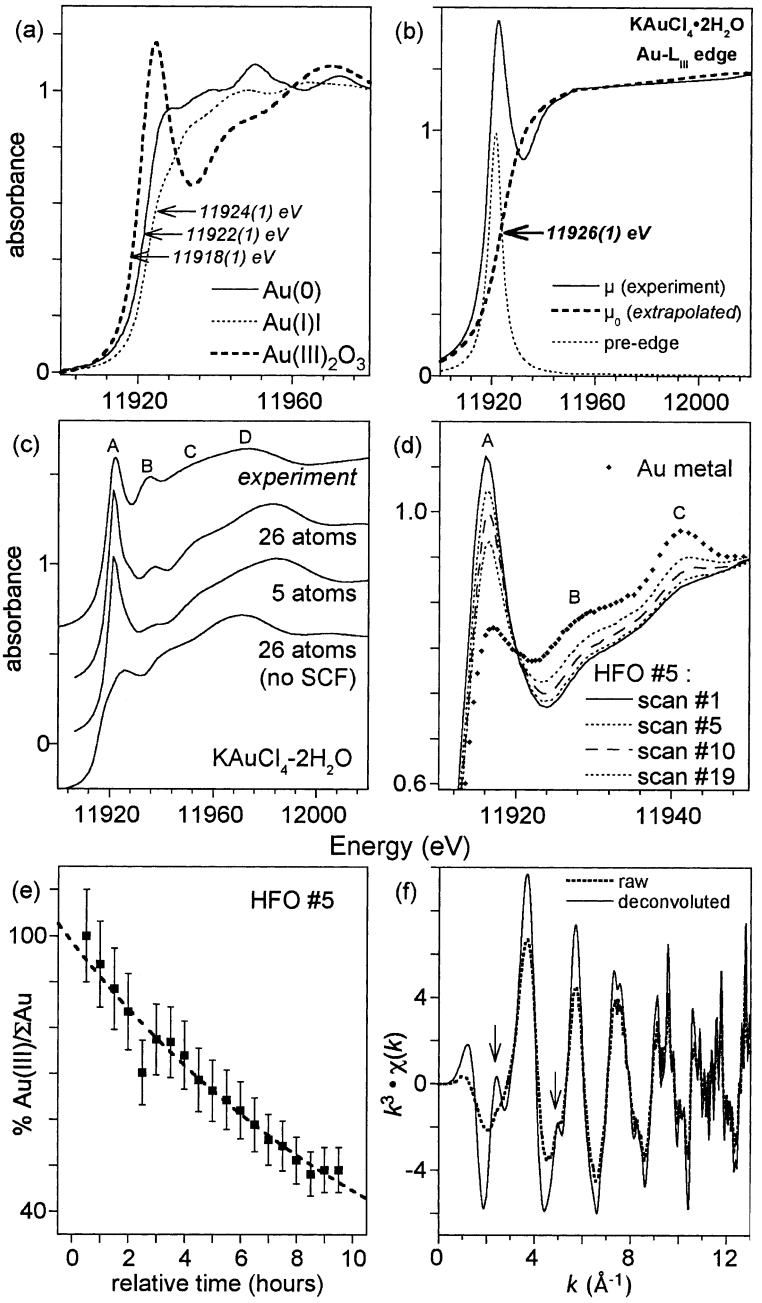

Fig. 1. (a) Au-L_{III} edge XANES spectra for Au-model compounds, showing the shift of the edge as a function of Au oxidation state. Note the relatively low energy for Au(III) (as in Au_2O_3); (b) the model of the edge, assuming a pseudo-Voigt for the "white-line (in fact, a preedge feature) and an arctangent for the edge jump; (c) theoretical XANES spectrum for $KAuCl_4$-$2H_2O$ calculated using Feff8.2, showing the need for self-consistent potentials (SCF) to model the "white line" (as a preedge feature, or feature A). All other XANES features are obtained for a limited number of atoms (convergence was reached for 26 atoms). Note that feature B is obtained for an $AuCl_4$ cluster ("5 atoms"), suggesting that it is a good spectroscopic signature for square-planar AuO_4 moieties; (d) example of an photo-reduction experiment performed on a Au(III)/ferrihydrite sorption sample collected at 290 K at SSRL; (e) photo-reduction kinetics, based on the two end members Au(III) and Au(0), estimated using principal component analysis and target reconstruction methods. Under these conditions, photo-reduction is observed to be negligible at 1 h or less of illumination by the incident X-ray beam; (f) spectral deconvolution of the EXAFS spectrum collected for a Au(III)/goethite sorption sample, assuming a core-hole lifetime of 4.5 eV. The deconvolution enhances discrete features (indicated by arrows) such as multi-electronic excitations at *k*-values close to those predicted by the GNXAS package (Benfield et al., 1994).

edge position for Au(III) appears to be shifted to lower energy (by ~ 2 eV) relative to Au(I). This unusual apparent shift is explained by noting that the "white line" of gold is actually an intense and poorly resolved preedge feature, as observed for TiO_4-bearing crystalline oxides (see Farges et al., 1996) or for Br-containing aqueous solutions (Filipponi, 2000). Based on this observation, a more accurate estimate of the position of the L_{III} edge for Au(III) is determined by fitting a pseudo-Voigt and an arctangent function to the proposed preedge feature and edge jump, respectively (Fig. 1b). Based on this model, the inflection point of that arctangent function is located at 11,926(1) eV in $KAuCl_4 \cdot 2H_2O$. The new, corrected edge position is 2 eV above that for Au(I) and 4 eV above that of metallic gold, in good agreement with shifts in edge positions for increasing oxidation states of other transition elements. Assuming this model is correct, this preedge feature can be related to electronic transitions from the initial 2p ground states of Au to the partially empty 5d final states, possibly partially hybridized by crystal-field effects. To support this model, ab inito XANES calculations at the Au-L_{III} edge in crystalline $KAuCl_4 \cdot 2H_2O$ were made using FEFF8 (version 8.20x8: Ankudinov et al., 1998) (Fig. 1c). We used self-consistent Hedin-Lunqvist potentials and the full multiple scattering (FMS) method, based on the crystal structure of $KAuCl_4 \cdot 2H_2O$ (Theobald and Omrani, 1980). The calculated spectra show that the "white line" feature is reproduced only if self-consistent potentials are used within a cluster of at least 26 atoms around the central Au (cutoff radial distance of 5 Å). Analysis of the 12 self-consistency loops during this calculation showed that FEFF8 predicts a formal charge of + 0.4 for the central Au (the trivalent state being the nominal charge). This value is similar to the charge of + 0.54 predicted for Au in a square-planar complex of oxygens using 82% covalent character for the Au-O bond (calculated using Pauling electronegativities for Au and O) and a bond valence of 0.75 vu for the Au-O bond. As a result of this reduction in charge, the Fermi level is shifted by −5 eV, and the electronic transition to the first empty 5d levels is observed as an intense feature located 5 eV below the Fermi level for metallic gold. Using this reduced charge on the central Au, the FEFF8.2 calculation confirms that the L_{III} XANES of Au(III) is composed of an intense preedge feature with a natural width that prohibits straightforward determination of edge position.

2.6.2. Monitoring the photo-reduction of gold

Oxidized species of gold (e.g., Au(I) and Au(III)) are highly sensitive to energetic photons and may undergo photo-reduction. X-ray beam-induced photo-reduction could, therefore, interfere with the objective of our study: to determine the nature of Au(III) adsorption complexes on common soil mineral surfaces. In our samples, we observed that the photo-reduction of Au(III) resulted in the formation of metallic gold, which has distinct XANES and EXAFS features as compared to Au(III), including the edge position as explained above. Therefore, we conducted deliberate photo-reduction experiments under controlled conditions of X-ray photon flux and time on a variety of samples (mostly Au(III) adsorbed on goethite and ferrihydrite) to monitor these effects. The progressive reduction of gold can easily be identified by a slight, but constant decrease in the normalized intensity of the "white line," and by a shift in its position by ~ +1 eV (Fig. 1d). Based on these results, the amount of trivalent gold that underwent photo-reduction was estimated from a principal component analysis (PCA) to be ~50 atom% of the initial gold after 10 h of synchrotron X-ray beam illumination at SSRL on beam line 4–3 (Fig. 1e). Fortunately, by using a He-cooled cryostat, photo-reduction could be reduced to a level not detectable by XAFS methods over the time frame of these experiments. Similarly, photo-reduction was not detectable in EXAFS spectra taken on the EXAFS2 beamline at LURE, while only a few minutes of exposure was long enough to photo-reduce gold on an undulator beamline on a third generation synchrotron source such as the ESRF or APS.

2.6.3. Multi-electron excitations

Benfield et al. (1994) have identified two weak, but significant, multi-electron excitations (MEE) in the Au-L_{III} edge EXAFS region in crystalline $KAuCl_4 \cdot 2H_2O$. The most important one (labeled [2p5f] in their paper) is a 5f → nε electronic transition, promoted by the more probable 2p → nε transition (the origin of the main L_{III} edge). This additional transition will, therefore, be present in any EXAFS spectrum collected at the L_{III} edge of Au(III). Despite the fact that such a transition should have the shape of a weak absorption edge, it is present as an interfering shoulder near 5.5 $Å^{-1}$ in the spectrum of $KAuCl_4 \cdot 2H_2O$. Such a feature cannot be properly modeled using most XAFS software packages, with the notable exception of the GNXAS code (Filipponi et al., 1991, Filipponi, 2000) or Viper (Klementiev, 2000). Using Viper, we deconvoluted a normalized EXAFS spectrum for a sample of goethite with adsorbed Au (sample G5, pH 7, discussed later), assuming the core-hole lifetime broadening for Au at the L_{III} edge to be 4.5 eV (Krause and Oliver, 1979) (Fig. 1f). Core-hole lifetime deconvolution strongly affects the *k*-region of the EXAFS near 2.4 and 5.0 $Å^{-1}$, in fair agreement with Benfield et al. (1994) on Au(III)-bearing model compounds. Consistent with previous studies (e.g., see Solera et al., 1995), we observed that the influence of these features on the way that backgrounds and atomic absorption are fitted to EXAFS spectra is limited to some distortion in the normalizing baseline. Such errors in the baseline may result in "low frequencies" in the Fourier Transform, which are located well before the first-neighbor contribution (i.e., below 1 Å in the FT). However, we found that the EXAFS-derived parameters for model compounds (such as Au_2O_3, $AuCl_3$ or $KAuCl_4 \cdot 2H_2O$) are not significantly affected by these MEE features, even though the calculated model is not accurate in the 5.0–5.5 Å region where MEE occurs.

2.6.4. Multiple scattering interferences

Multiple-scattering (MS) paths of the photoelectron are significant in the case of Au(III) located in a square-planar geometry (Farges et al., 1993; Benfield et al., 1994). Because of these extra paths, MS contributions related to the C_{4V} geometry can be observed in the FTs at higher R-values than the regular, more probable single-scattering (SS) paths (i.e., the main contribution related to first neighbors in the FT). Using the FEFF

code (versions 7.02 and 8.25: Ankudinov et al., 1998), we were able to estimate the magnitude of these effects in the XANES and EXAFS spectra. As outlined previously (Farges et al., 1993; Benfield et al., 1994), a MS feature related to O/Cl first neighbors can be observed in the XANES spectra of most Au(III)-bearing compounds, as confirmed by ab initio full multiple-scattering XANES calculations (using FEFF8.2 5; see Fig. 1c). Therefore, this feature is a qualitative, but straightforward, preliminary indication of Au(III) speciation in the unknown samples. In the case of Cl first neighbors (as in $KAuCl_4 \cdot 2H_2O$), this feature is intense and located near 11,935 eV. In the case of oxygen ligands around Au(III), this feature is much smaller and shifted by 9 eV to higher energy (11,944 eV). Similarly, the position of the "white line" is shifted from 11,922 to 11,924 eV from gold-chlorides to gold-oxides, in agreement with observations at the L_{III} edge of Pt in glasses (Farges et al., 1999). The greater atomic number and ionic radius of Cl relative to oxygen results in larger backscattering amplitude and larger effective multiple-scattering distance, respectively. Hence, both a higher intensity for this feature and a shift toward lower energies (as compared to oxygen ligands) are predicted (because $E \alpha 1/R^2$, in which E and R are the energy position of the feature considered and an effective distance R). This prediction is consistent with the XANES measurements on Au-containing model compounds. With FEFF, we estimated the relative importance of MS contributions to the EXAFS region in several model compounds (see Figs. 2a–c). These calculations show, that among the many possible photoelectron scattering paths, two particular paths contribute significantly (see Berrodier, 2001, for details). First, a triangular order-3 path (i.e., Au→X→X→Au, with X = O or Cl) is predicted, with an effective distance of 3.4 Å and 3.9 Å for O and Cl neighbors, respectively (its relative importance compared to the single-scattering Au→X→Au is 10%). Second, an order-3 path (i.e., Au→X→X→Au, with X = O or Cl) is observed with an effective distance of 4.0 Å and 4.6 Å for O and Cl neighbors, respectively (its relative importance compared to the single-scattering Au→X→Au is 20%). Finally, an order-4 path (X 171 Au 171 X) is also noteworthy, with an effective distance of 4.0 and 4.6 Å for O and Cl neighbors, respectively (with a relative importance compared to the single-scattering Au→X→Au of 50%). The relative intensity of these MS contributions is enhanced in the presence of Cl first neighbors (instead of O), and in the case of square-planar environments with only small distortions (as in $KAuCl_4 \cdot 2H_2O$). The MS contributions near 3.4 Å might, therefore, interfere with the SS signal arising from next-nearest neighbors (Al/Fe) in (oxy)-hydroxides on which Au is adsorbed. Thus, all models of the medium-range environment of Au in these oxy-hydroxides included one or two extra contributions related to MS arising from first neighbors.

2.6.5. *Wavelet analysis of Au-L_{III} EXAFS spectra*

Wavelet analyses (see Muñoz et al., 2003, for a discussion of this method) was conducted for EXAFS spectra collected at the Au L_{III} edge in a number of Au(III)-bearing aqueous solutions and Au(III)/goethite adsorption sample (such as sample G6, synthesized at pH 7.9; see later). In brief, a wavelet diagram shows the (*k*,R) dependence of information derived from an EXAFS spectrum. Any increment in *k*-space (Δk) is represented as a function of the R-space ($\Delta(R+\Delta R)$) by infinitesimal FT analysis, and the third dimension is given by the modulus of each $\{\Delta k, \Delta(R+\Delta R)\}$ pixel component (Muñoz et al., 2003). Figure 3 shows the wavelet analysis performed on a sample of Au(III) adsorbed on goethite (Fig. 3b is a 3D view of the wavelet diagram presented in Fig. 3a). In this adsorption sample, Au is surrounded by oxygen first neighbors (no detectable chlorine first neighbors). Examination of Figure 3a shows that the single-scattering Au-O contribution has an edge crest that is horizontal in (*k*, R) space (the EXAFS frequency varies linearly with *k*). This suggests that few anharmonic effects affect the data. Furthermore, the oxygen first neighbors also generate some multiple-scattering features as suggested by the presence of a large feature in the $k = 3–6$ Å^{-1}, R = 3 Å region. From these MS features, one can infer from the EXAFS region that Au(III) occupies a square-planar geometry in the adsorption sample (FEFF MS calculations suggest that other possible geometries, like T_d, do not induce much MS). Also, for the sample with Au(III) adsorbed on goethite, the EXAFS spec-

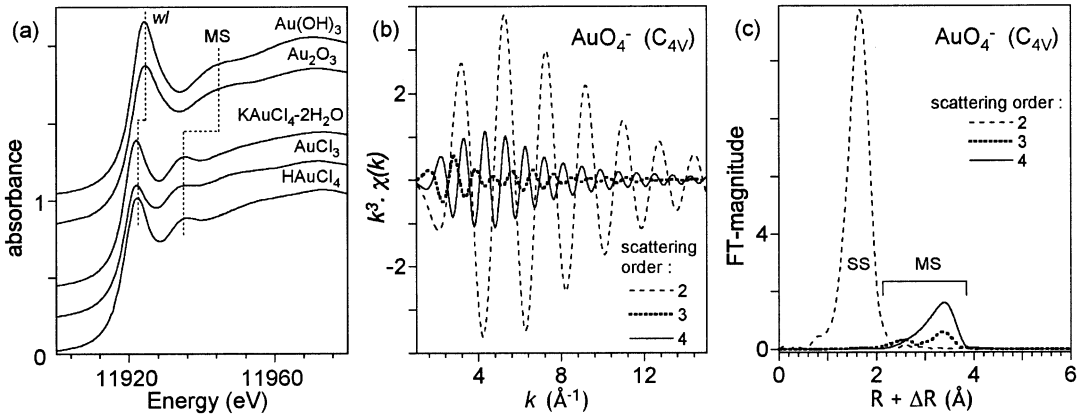

Fig. 2. (a) left: XANES for selected model compounds, showing the shift of the "white line" (w-l) and the multiple-scattering (MS) feature related to first neighbors around Au; (b) middle: theoretical calculations (FEFF8.2) of the EXAFS signal for single-scattering (order 2) and multiple scattering (orders 3 and 4) arising from an AuO_4^- cluster; (c) right: FTs of the EXAFS spectra presented in (b), showing the relative importance of MS paths as compared to SS paths.

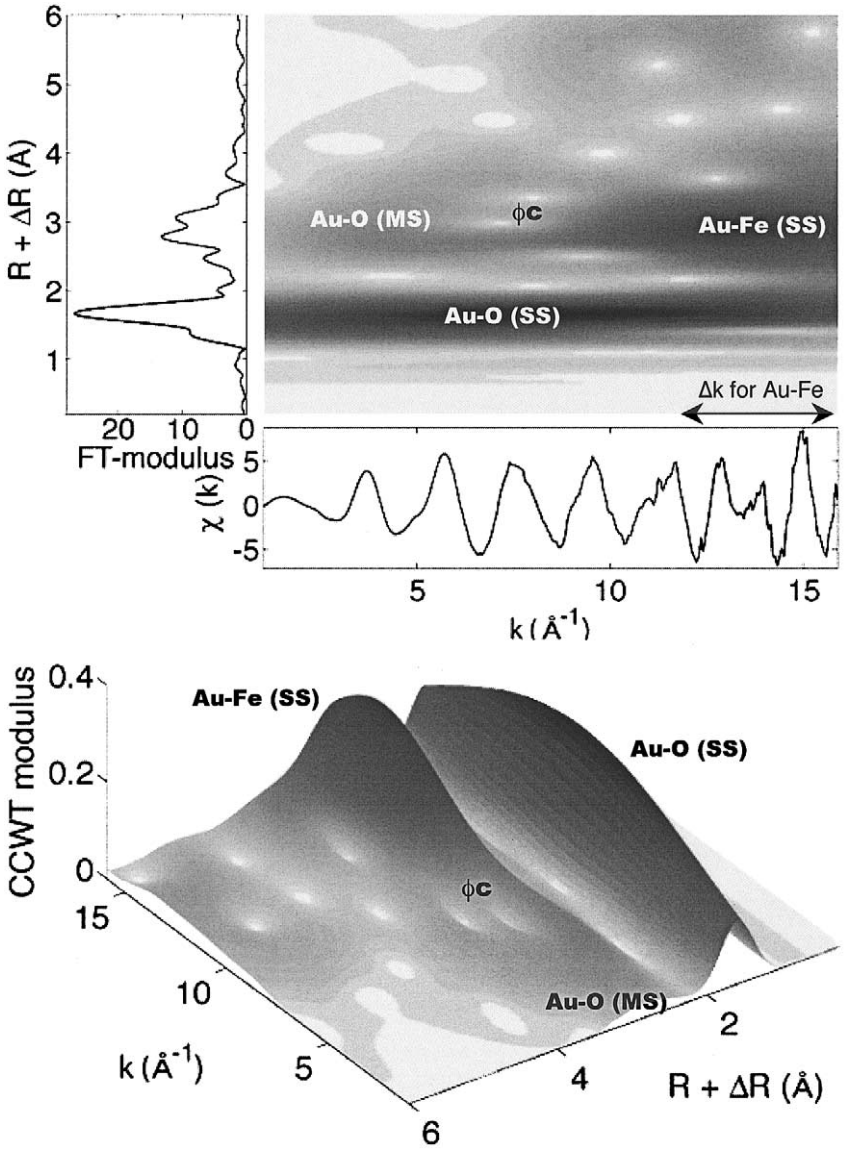

Fig. 3. (a) left: Wavelet Transform (WT) plot for an Au(III)-bearing goethite sample (sample G6-pH 7.9), with the momentum vector (k) plotted along the abscissa and the direct space distance ($R+\Delta R$, i.e., uncorrected for phase-shifts, ϕ) plotted along the ordinate. (b) right: reconstructed surface of the WT, using false gray levels for the WT magnitude. The three types of contributions around Au(III) can be visualized easily and consist of (1) harmonic Au-O pair correlations, (2) single and multiple-scattering Au-O features, and (3) Au-Fe next nearest neighbor contributions (important to k values of 15.5 Å). The modeled edge for the first neighbors (dotted line) is "horizontal enough" to indicate an harmonic Au-O shell of neighbors.

trum was collected out to $k = 15.5$ Å^{-1}. For the Au-O pair correlation, however, the collection of EXAFS data to $k = 13$ Å^{-1} would have been statistically sufficient, as more than 99% of the integrated area for the Au-O contribution is observed as a single large spot in the $k = 1$–15 Å^{-1}; $(R+\Delta R) = 1.5$ Å region (Fig. 3b). In order for this last statement to be valid, the EXAFS spectrum was not convoluted with the Kaiser-Bessel window function before being wavelet-transformed, to avoid artificial minimization of the amplitude of the experimental EXAFS spectrum at its borders (near $k = 1$ and 15 Å^{-1}). Second-neighbor Fe can be observed near $(R+\Delta R) = 3$ Å in the wavelet transform. For these second neighbors, the majority of their EXAFS signal is observed for k-values between13 and 16 Å^{-1}. If EXAFS data had been collected only to $k = 13$ Å^{-1} (as is often done in many EXAFS experiments, typically because of the significant extra time required for collecting higher k-range EXAFS data and the limited amount of beam time allocated for most experiments at synchrotron light sources), the structural information for these next-nearest neighbors would have been much less robust (only 1/4 of the actual Au-Fe contribution would have been measured).

Finally, the EXAFS contribution arising from these second neighbors interferes strongly with the MS features from the O first neighbors. This is true because the Au-O (MS) and the

Au-Fe (SS) occur at nearly the same (R+ϕ) values. As a result, a large destructive interference occurs between the EXAFS contributions from these two sources, which can be viewed (as "ϕc" Fig. 3b) between 9 and 11 Å^{-1} as a "hole" in the wavelet transform magnitude. As a consequence, the FT-magnitude does not show these details, which makes any FT-peak assignment unreliable. Although the structural environments for Au presented in this paper are based on wavelet transforms, for clarity, we present the corresponding FTs. Figure 4 shows typical fits computed for two Au-bearing goethites, in which we fit first oxygen neighbors (single- and multiple-scattering contribution of orders 3 and 4) as well as two Au-Fe shells of next nearest neighbors. However, we will show that these distant Au-Fe contributions (such as that presented in Fig. 4) are, most likely, modeled too simplistically. However, current EXAFS software does not appropriately compute disorder effects in the medium-range environment around any type of absorbing atom (usually resulting in severely underestimated distances and number of neighbors: see Crozier et al., 1988). We will make use of reverse Monte Carlo models to demonstrate how disorder effects impact any modeling of the medium-range environment around an atom that is computed using conventional EXAFS data analysis methods (such as that presented in Fig. 4).

3. RESULTS

3.1. Goethites

3.1.1. Raman scattering spectroscopy of Au-containing solutions

The spectral region showing stretching modes of the Au-Cl and Au-OH bonds is between 300 and 400 cm^{-1} (see Fig. 5a). The intensity of these bands decreases dramatically with increasing pH (Peck et al., 1991; Murphy et al., 1998). At pH 2, deconvolution of this spectral region resulted in two bands (325 and 347 cm^{-1}) that were assigned to vibrational modes related to the $AuCl_4^-$ moiety. These two Raman bands have been calculated from first principles to occur at 323 and 353 cm^{-1} (Tossel, 1996), which is consistent with the results of Peck et al. (1991) and Murphy et al. (1998) who observed bands at 324 and 347 cm^{-1} and at 325 and 348 cm^{-1}, respectively, for similar Au-bearing solutions at pH 2. Another small contribution located at 333–335 cm^{-1} was assigned to vibrational modes related to the $AuCl_3OH^-$ moiety. The vibrations characteristic of this moiety are predicted to occur at 324, 341, and 352 cm^{-1} (Tossel, 1996). At higher pH (4), these three bands are again observed in the solutions studied. However, the relative intensity of the band related to the $AuCl_3OH^-$ species is much higher as compared to that at pH 2. At pH 6, two bands are detected, which are located at 338 and 354 cm^{-1}. These Raman bands are characteristic of the $AuCl_2OH_2^-$ moiety, following the Raman studies conducted by Peck et al. (1991) and Murphy et al. (1998), who observed these bands at 337 and 354 cm^{-1}. However, Tossell (1996) predicted that these bands should be located at slightly lower energies, namely 317 and 328 cm^{-1}. At pH 7, two bands are observed at 338 and 355 cm^{-1}, and their intensity is much lower than those measured for Au-bearing solutions at pH 6 (and the signal-to-noise ratio is dramatically lower). The band at 356 cm^{-1} was assigned by Peck et al. (1991) and Murphy et al. (1998) to the $AuClOH_3^-$ moiety, which differs quite significantly from the prediction of Tossel (1996) (321 cm^{-1}). As theoretical calculations of Raman scattering are still subject to some computational assumptions, we follow the empirical assignments of Peck et al. (1991) and Murphy et al. (1998) for the various bands associated with Au-O and Au-Cl vibrations. Thus, our Raman scattering study suggests that our starting Au-bearing solutions show gold speciation consistent with those of past studies (Peck et al., 1991; Murphy et al., 1998), although the Au/Cl concentrations are not fully comparable.

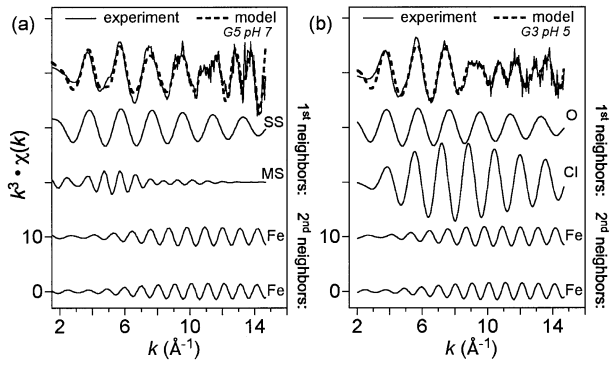

Fig. 4. Example of EXAFS models calculated for two goethites (samples "G3" and "G5") at the Au-L_{III} edge. When Au shows a mixed O/Cl environment (left), multiple scattering is less significant (as observed directly using wavelet analysis) and, therefore, can be excluded from the model. In contrast, samples equilibrated at higher pH (right) show single-(SS), and multiple-scattering (MS) contributions arising from oxygen first neighbors, both of which are significant. For both models, two shells of neighboring Fe (near 3.1 and 3.3 Å) are required to model the experimental data (top curves).

3.1.2. XANES for the solutions, before and after uptake

The Au-L_{III} XANES spectra of gold-bearing solutions confirm the change in Au-speciation with pH (with Au remaining trivalent in all cases studied). As seen in Figure 5b, for solutions containing 0.01 mol/L [Cl] and 3.45 $\times$ 10^{-3} M [Au] (pH $<$ 5), the Au-L_{III} edge XANES spectra have multiple-scattering (MS) features located at 11,940 eV, typical of the $AuCl_4^-$ moiety (see Farges et al., 1993). In contrast, at higher pH values (>5), the XANES spectra for solutions show MS features related to O-rich environments around Au(III). The same trends are observed for solutions containing 0.1 mol/L [Cl] and 9.5 $\times$ 10^{-4} M [Au] (Fig. 5c). We also collected Au-L_{III} edge XANES spectra for selected supernatants (0.01 mol/L [Cl] and 3.45 $\times$ 10^{-3} M [Au]), after Au uptake by goethite (Fig. 5d). In this series of solutions, there are no significant spectral differences relative to the corresponding initial solutions, suggesting that no significant change in the speciation of gold occurred during uptake (e.g., no evidence for metallic gold formation).

3.1.3. XANES of the Au(III)-bearing goethites

The Au-L_{III} XANES spectra for Au adsorbed on all goethite samples studied here show an intense "white line" that we attribute to an intense preedge feature, suggesting the presence of Au(III). This feature for all Au(III)/goethite

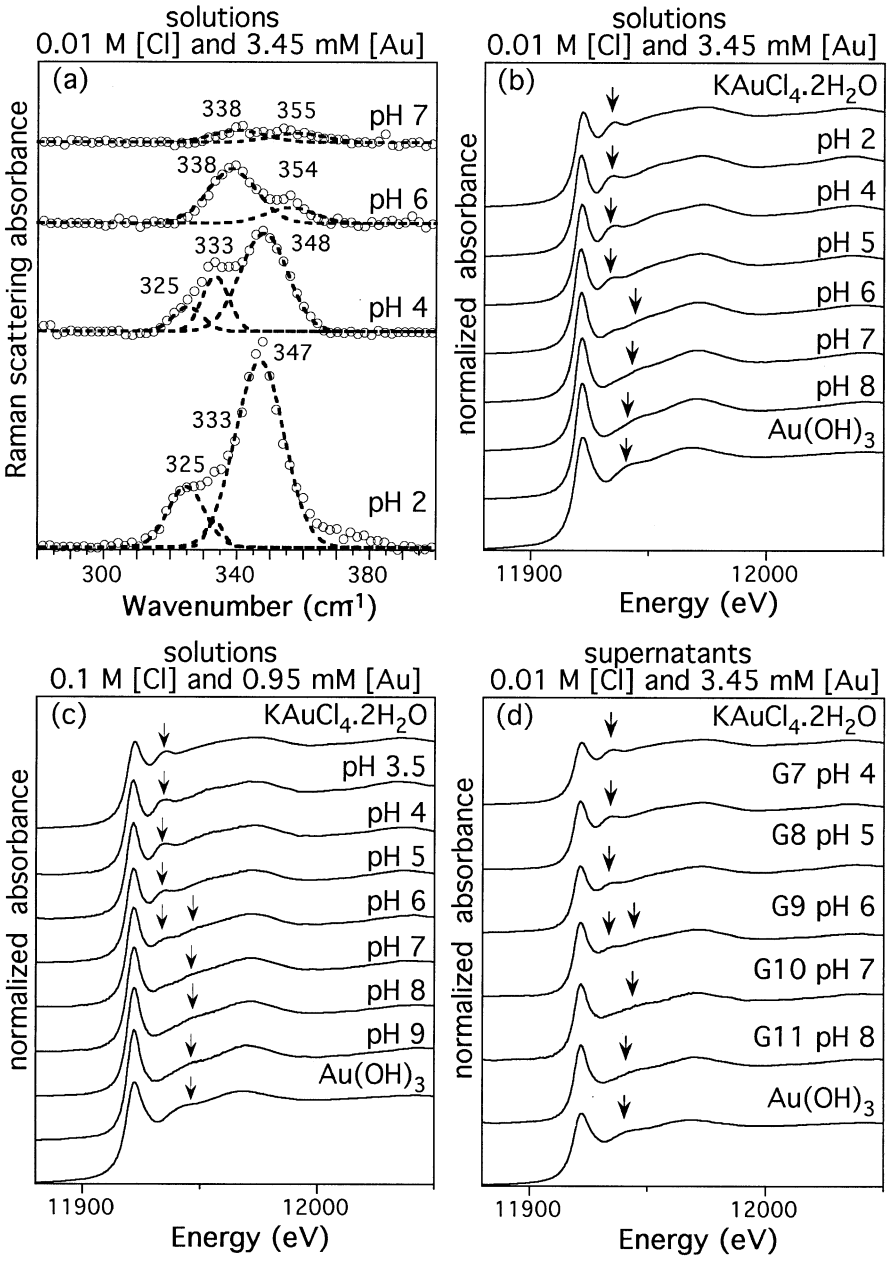

Fig. 5. (a) Raman spectra of a gold chloride solution with 0.01 mol/L [Cl] and 3.45 mM [Au]; (b) XANES spectra of a gold chloride solution with 0.01 mol/L [Cl] and 3.45 mM [Au]; (c) XANES spectra of a gold chloride solution with 0.1 mol/L [Cl] and 0.95 mM [Au]; (d) XANES spectra of gold in a supernatant with initial conditions of 0.01 mol/L [Cl] and 3.45 mM [Au].

adsorption samples has the same position and relative intensity as that observed in $KAuCl_4 \cdot 2H_2O$ and Au_2O_3, suggesting that X-ray beam-induced photo-reduction of Au(III) was minimum for all samples (Figs. 6a–c). Thus, Au remained in the trivalent state in most samples during XAFS data collection. At high pH synthesis values (≥6), the Au-L_{III} XANES spectra of gold adsorbed on goethite are similar to that for crystalline Au_2O_3 (i.e., similar MS feature), suggesting the presence of AuO_4 units in these samples. In contrast, at low pH values, the XANES spectra show two MS features, suggesting the presence of a mixed O/Cl environment around Au. When compared to the solutions before and after adsorption (Figs. 5c,d), there are clear differences in the XANES for acidic solutions, related to the MS feature located near 11,940 eV. These spectral differences suggest that large changes in the coordination environment of Au(III) have occurred as a result of adsorption at the mineral/water interface. These changes suggest that more O than Cl ligands are present around Au(III) on the goethite surface (as compared to the corresponding aqueous Au). However, these changes are minor for most of the samples (i.e., at pH above 6).

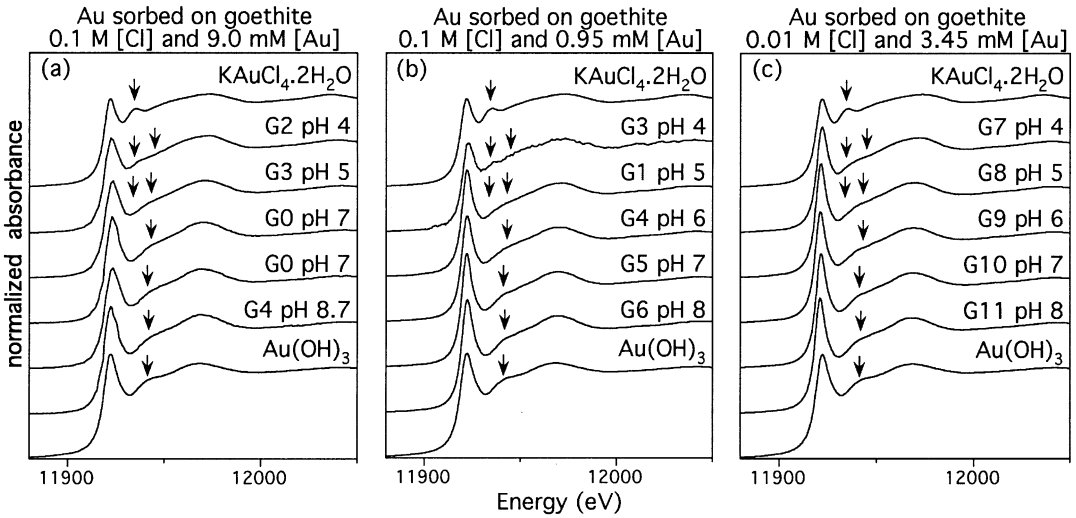

Fig. 6. (a) XANES spectra of gold adsorbed on goethite from a solution containing 0.1 mol/L [Cl] and 9.0 mM [Au]; (b) XANES spectra of gold adsorbed on goethite from a solution containing 0.1 mol/L [Cl] and 0.95 mM [Au]; (c) XANES spectra of gold adsorbed on goethite from a solution containing 0.01 mol/L [Cl] and 3.45 mM [Au]. The arrows indicate the presence of the MS features related to either Cl and O-first neighbors (these features are indicated as their observation requires zooming and analysis of first derivatives that cannot be detailed here; see Farges et al., 1993, for more information).

3.1.4. EXAFS for the first neighbors

Figure 7a shows k^3-weighted, background-subtracted EXAFS spectra for selected Au-bearing goethites, and the corresponding FTs are shown in Figure 7b. In Au(III)/goethite adsorption samples, the FT shows one main contribution for first neighbors, located at the same distance as for Au(III) oxide and chloride model compounds, suggesting the presence of Au-O/Cl bonds, depending on the sample synthesis conditions. A low pH, this first-neighbor contribution splits into two components (Fig. 7b,d), related to the presence of a shell of first neighbors containing both O and Cl. Table 1 gives the refined EXAFS parameters for these Au-O/Cl contributions (see Fig. 8) for the best fits obtained for these spectra). In all samples, the mean Au-O and Au-Cl distances (when measurable) are about the same, i.e., 2.00(2) and 2.28(2) Å, respectively. These distances are typical of 4-coordinated Ausquare-planar complexes (see Farges et al., 1993). The AuX_4 (with X=O and/or Cl) polyhedra show very little radial distortion, as indicated by a Debye-Waller factor σ^2 and an anharmonic parameter C_3 (relative to respective model compounds) that are near zero. In addition, the number of O/Cl first neighbors around Au depends on both the pH and the Cl-concentration in the original Au-bearing solution. As compared to the solutions, the relative number of oxygen first neighbors is much greater for the Au(III)/goethite adsorption samples ($AuCl_4^-$ moieties were not observed in any of these samples).

3.1.5. EXAFS for the next-nearest neighbors and MS interferences

The FT for the various samples of gold-bearing goethites show three contributions arising from Fe second and third neighbors as well as the MS contribution from the square-planar moieties. Results of the modeling of these three contributions for selected goethites are similar (within errors). In all samples, the Au-Fe distances are observed near 3.1(1) and 3.3(1) Å (distances corrected for phase-shifts). Only, the relative magnitude of such contributions varies (higher in goethite, lower in HFOs). In fact, disorder effects in the medium-range environment of Au on goethite are potentially very large (due to goethite surface relaxation and the presence of an amorphous fluid, water, which "randomize" the way gold atoms adsorb on the surface. Because of these potential artifacts, the use of standard EXAFS modeling method is not recommended because the so-called "harmonic approximation" is no longer valid (hence, EXAFS data analysis software lacking anharmonic analysis capabilities should not be used for analyzing such data). If disorder effects are not taken into account, the distances and number of neighbors obtained in EXAFS analysis can be severely underestimated (up to 50%: see, e.g., Crozier et al., 1988; Farges and Brown, 1996). The problem encountered in the present study is that currently available anharmonic methods are difficult to apply to the adsorption of metal cations on an oxide surface because the magnitude and shape of the distance distribution in the medium-range environment around the adsorbed cation (here, Au) is unknown. Other methods have to be used to obtain a more robust picture of disorder effects. To address this issue, we present Reverse Monte Carlo simulations in the discussion section that confirm the presence of severe radial disorder around Au on the surface of goethite. These simulations indicate that quantification of the next-nearest neighbor environment of iron around Au cannot be modeled accurately using conventional EXAFS data analysis methods. As a consequence, we will not present the EXAFS-derived structural information obtained for Au-Fe pairs in the different goethite samples (nor that for Au-Al pairs in boehmite or Au-Fe pairs in ferrihydrites) because the various models converged to similar Au-Fe distances within errors (see Fig. 4) for a example of detailed analysis).

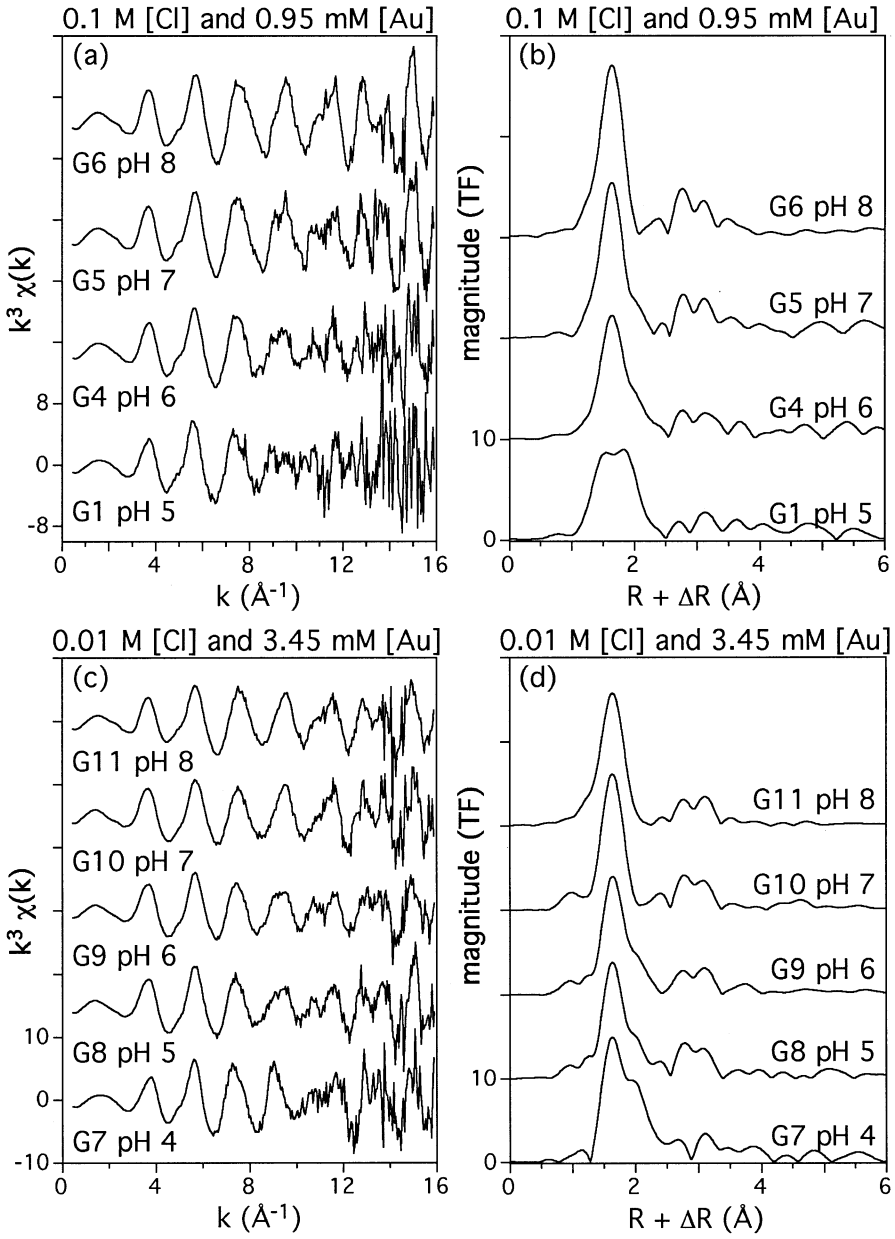

Fig. 7. (a) k^3-weighted EXAFS spectra of gold adsorbed on goethite from a solution containing 0.1 mol/L [Cl] and 0.95 mM [Au]; (b) Fourier Transform of the k^3-weighted EXAFS spectra of gold adsorbed on goethite from a solution containing 0.1 mol/L [Cl] and 0.95 mM [Au]; (c) k^3-weighted EXAFS spectra of gold adsorbed on goethite from a solution containing 0.01 mol/L [Cl] and 3.45 mM [Au]; (d) Fourier Transform of the k^3-weighted EXAFS spectra of gold adsorbed on goethite from a solution containing 0.01 mol/L [Cl] and 3.45 mM [Au].

3.2. Au(III)/boehmite adsorption samples

The Au-L_{III} XANES spectra of Au(III)/boehmite adsorption samples (pH 6 to 8: Fig. 9a) are similar to that measured for crystalline Au_2O_3, which suggests an environment similar to that in AuO_4 units (including also $Au(OH)_4$, as protons do not contribute significantly to XAFS spectra). These XANES results are consistent with the analysis of the EXAFS spectra (Fig. 9b) and their corresponding FTs (Fig. 9c). For both series of Au(III)/boehmite adsorption samples (the first series was prepared from solutions containing 0.1 mol/L [Cl] and 9.0 $\times 10^{-5}$ M [Au]; the second series was prepared from solutions containing 0.01 mol/L [Cl] and 4.2 $\times 10^{-5}$ M [Au]), we observe only O first neighbors in the short-range environment of Au, with EXAFS-derived structural parameters (see Fig. 9d and Table 2) consistent with fairly regular square-planar Au-O_4 moieties. In these samples, the FTs of the EXAFS spectra (Figs. 9b,c) also show two contributions, which arise from Al second neighbors located at 3.0 (1) and 3.2 (1) Å (distance are corrected for phase-shifts). A third contribution, related to MS inside the AuO_4 units is also observed near 4.0 (1) Å. In some

Table 1. Synthesis conditions and EXAFS parameters for gold adsorbed on goethites.

Sample	pH[a]	[Au][b] (%)	[Au][c] (mmol/m^2)	Type and number of first neighbors		d(Au-X) (Å)	$\Delta\sigma^2 \times 10^{-3}$ (Å^2)	$\Delta C_3 \times 10^{-4}$ (Å^3)	ΔE_0 (eV)
				0.1 M [Cl] and 9.0 mM [Au]					
G2	4.10	1.09	0.697	O	2.1	2.00	0	0	0
				Cl	2.1	2.31	0	0	0
G3	5.05	2.41	1.53	O	4.4	2.00	0	0	0
				Cl	0.4	2.29	0	0	0
G1	6.02	5.29	0.335	O	4.1	1.99	0	0	−0.9
G0	7.15	n.m.[d]	n.m.	O	4.1	2.00	0	0	−0.2
G4	8.70	4.80	0.304	O	3.8	1.99	0	0	−1.2
				0.1 M [Cl] and 0.95 mM [Au]					
G1	5.00	0.913	0.058	O	2.33	2.01	0	0	−3.0
				Cl	1.90	2.27	0	0	+2.0
G4	5.85	1.61	0.102	O	4.12	2.03	0	0	0.5
				Cl	0.10	2.29	0	0	+3.0
				or					
				O	3.70	2.02	0	0	−1.5
G5	7.01	1.42	0.090	O	4.44	2.01	0	0	−1.1
G6	7.90	1.44	0.091	O	3.98	2.00	0	0	−2.2
				0.01 M [Cl] and 3.45 mM [Au]					
G7	4.1	1.86	0.118	O	3.23	2.01	0	5	−2.6
				Cl	1.08	2.30	0	7	+2.3
G8	4.82	3.40	0.215	O	3.71	2.01	0	0	−0.2
				Cl	1.09	2.28	0	0	+3.0
G9	6.00	3.14	0.199	O	4.22	1.99	0	0	−3.0
G10	6.94	3.90	0.247	O	3.82	2.01	0	0	−1.3
G11	7.93	3.46	0.219	O	3.98	2.00	0	0	−1.7
Error	0.02	0.01	0.003		0.5	0.02	0.001	0.0001	

[a] pH after equilibration between the solid and the solution.
[b] [Au] concentration in the solid phase in % (*i.e.*, g of Au per 100 g dry weight goethite).
[c] Calculated using specific surface areas from BET experiments (i.e., 79 m^{2}g^{-1}).
[d] n.m. = not measured.

boehmite samples, in which X-ray beam-induced photo-reduction was always significant, a contribution arising from metallic gold is observed near 2.87 (5) Å.

3.3. Au(III)/ferrihydrite adsorption samples

Different Au(III)/ferrihydrite adsorption samples were prepared as a function of pH (see Table 1 for synthesis details for the three series of HFO adsorption samples investigated). Two series of HFOs were synthesized using iron chloride starting materials, and three series of HFOs were prepared from iron nitrate starting materials. The XAFS-derived structural details of the Au(III) adsorption products are given below.

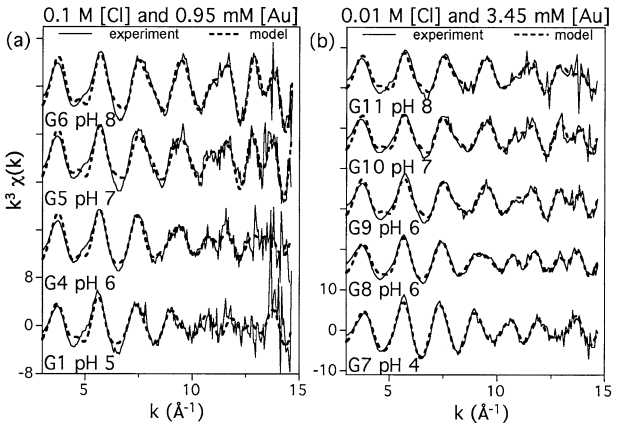

Fig. 8. Fits of k^3-weighted EXAFS spectra for gold adsorbed on goethite from a solution containing 0.1 mol/L [Cl] and 0.95 mM [Au]; (b) Fits of k^3-weighted EXAFS spectra for gold adsorbed on goethite from a solution containing 0.01 mol/L [Cl] and 3.45 mM [Au].

3.3.1. *Local environment of Au(III) adsorbed on HFOs synthesized from iron nitrate*

As for the Au(III)/goethite adsorption samples, the Au-L_{III} edges collected for various types of Au(III)/HFO adsorption samples do not show any significant changes in energy position and white line height as compared to those for Au(III)-models compounds (see Figs. 10a, 11a, 12a), suggesting that gold adsorbed on these HFO samples is dominantly Au(III). Gold adsorption experiments performed on natural HFOs resulted in the presence of dominant amounts of nano-crystallized metallic gold (the XANES spectra are not reported here, see Berrodier, 2001, for details); we attribute this metallic gold to the presence of reducing organic matter as evidenced by IR spectroscopy in these natural HFO materials from the Reunion Island (IR spectra not shown).

At high pH values (≥6), the Au-L_{III} edge XANES spectra of Au(III)/HFO adsorption samples are similar to that for crystalline Au_2O_3, suggesting that the first-shell coordination environment around Au(III) in the adsorption samples consists of dominantly oxygens ligands arranged in a square-planar geometry. In contrast, for adsorption samples synthesized at more

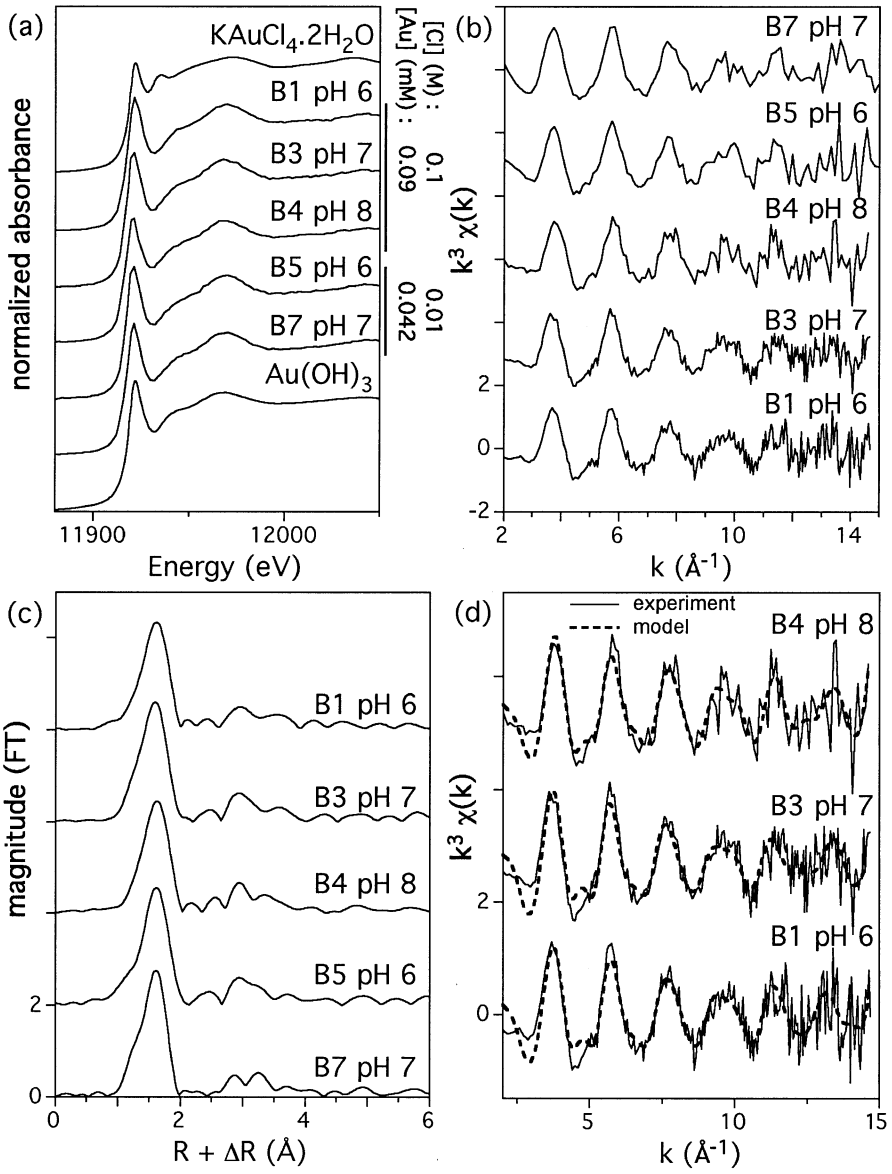

Fig. 9. (a) XANES spectra of gold adsorbed on boehmite from solutions containing 0.1 mol/L [Cl] and 9.0×10^{-5} M [Au] and 0.01 mol/L [Cl] and 4.2×10^{-5} M [Au]; (b) k^3-weighted EXAFS spectra for gold adsorbed on boehmite; (c) Fourier Transform of the k^3-weighted EXAFS spectra of gold adsorbed on boehmite; (d) Fits of k^3-weighted EXAFS spectra for gold adsorbed on boehmite.

acidic pHs (0.35 mol/L [Cl], pH $\leq$ 5), the Au L_{III}-edge XANES spectra indicate a mixed Cl/O environment around gold (still having C_{4v} point symmetry). For Au(III)/HFO adsorption samples prepared with a 0.02 mol/L [Cl] gold-bearing solution, chloride ligands are detected only at pH 4. For the series of Au(III)/HFO adsorption samples equilibrated with a 0.02 mol/L [Cl] gold-bearing solution, a mixed O/Cl environment is also detected at pH 3.85, whereas only oxygen ligands are present around Au at pH 6.2 and 7.4.

Selected EXAFS spectra for two series of Au(III)/HFO adsorption samples (0.35 mol/L [Cl] and 3.0×10^{-3} M [Au], 0.02 mol/L [Cl] and 3.0×10^{-3} M [Au]) and their corresponding FTs are presented in Figures 10b,c. Results of the least-square fitting of the FT-filtered EXAFS spectra for the first shell of neighbors around Au in our Au(III)/HFO adsorption samples are reported in Table 3 and Figure 10d. At pH 4 and for 0.35 mol/L [Cl], a mixed O/Cl environment around gold is observed with $\sim$ 2 oxygen atoms and $\sim$ 2 chlorine atoms ($\sim$3 oxygen atoms and $\sim$1 chlorine atom at pH 5.) At pH values of 7.9 and 9.4, only AuO_4 units are detected (which includes $Au(OH)_4$ moieties as well). The average Au-O/Cl distances were refined at 2.00(2) and 2.28(3) Å, respectively. These distances are close to those observed for Au-O and Au-Cl in model compounds (Au_2O_3 and $KAuCl_4 \cdot 2H_2O$). As for the Au(III)/goethite and Au(III)/boehmite adsorption samples, these AuX_4 (with X = O and/or Cl) moieties show small (if not zero) values for the σ^2 and C_3 values (relative to model compounds), suggesting very limited disorder and anharmonicity.

Table 2. Synthesis conditions and EXAFS parameters for gold adsorbed on boehmite.

Sample	pH[a]	[Au][b] (ppm)	[Au][c] (mmol/m^2)	Type and number of first neighbors		d(Au-X) (Å)	$\Delta\sigma^2 \times 10^{-3}$ (Å^2)	$\Delta C_3 \times 10^{-4}$ (Å^3)	ΔE_0 (eV)
				0.1 M [Cl] and 9.0 10^{-5} M [Au]					
B1	6.14	275	0.431	O	4.5	1.99	−1.5	0	−2.2
B3	7.0	214	0.337	O	4.5	1.99	−1.6	0	−2.7
B4	7.96	186	0.294	O	4.3	1.99	−1.7	0	0.9
				0.01 M [Cl] and 4.2 10^{-5} M [Au]					
B5	6.02	205	0.325	O	4.0	1.99	−2.1	0	−2.0
B7	7.05	198	0.312	O	4.5	1.99	−1.7	0	−1.5
error	0.02	5	0.003		0.5	0.02	0.001	0.0001	

[a] pH after equilibration between the solid and the solution.
[b] [Au] concentration in the solid phase in % (i.e., g of Au per 100g dry weight boehmite).
[c] Calculated using specific surface areas from BET experiments (i.e., 3.2 m^2 g^{-1}).

At pH 3.85 (0.017 mol/L [Cl] and 3.0×10^{-3} M [Au]), a mixed O/Cl environment (~ 3/1) is detected, whereas only O first neighbors are detected at higher pH values (see Table 3 and Figs. 10b–d).

We also tested the effect of keeping the [Au]/[Cl] ratio constant and increasing [Au] and [Cl], (the two series studied were: 0.35 mol/L [Cl] and 3.0×10^{-3} M [Au], and 0.6 mol/L [Cl] and 6.0×10^{-3} M [Au]). The XAFS experiments conducted for the most concentrated Au(III)/HFO adsorption samples yielded results consistent with those of the more dilute Au(III)/HFO adsorption samples. Also, the Au(III)/HFO adsorption sample prepared at pH 6.2 (0.6 mol/L [Cl]) has an EXAFS signal intermediate between that collected for the Au(III)/HFO sample at pH 5 (0.35 mol/L [Cl]) and the Au(III)/HFO sample at pH 7.9 (0.35 mol/L [Cl]), which corresponds to a 3/1 O/Cl environment. Similarly, at pH 4.5 (0.6 mol/L [Cl]) and at pH 4.2 (0.35 mol/L [Cl]), a mixed O/Cl environment (O/Cl: 2/2) is detected around Au. As for the other Au(III)/HFO samples, the Au-O and Au-Cl distances are constant irrespective of the moieties present: 2.00(2) and 2.28(3) Å, respectively. Again, the Debye-Waller factor, σ^2, and anharmonic parameter, C_3, (both relative to respective model compounds) are low, suggesting again there is little distortion of $AuOX_4$ (X=O/Cl) polyhedra in all the Au(III)/HFO adsorption samples examined. No significant Au-Au contributions could be detected (near 2.9 Å), which would be indicative of metallic gold (related to synthesis problems or photo-reduction events). These EXAFS results are consistent with the structural models derived from the Au-L_{III} XANES spectra.

3.3.2. *Local environment of Au(III) adsorbed on HFOs synthesized from iron chloride solutions*

Except for the Au(III)/HFO samples 1 and 5 which show evidence for significant photo-reduction of Au (Fig. 12a), all other Au(III)/HFO adsorption samples prepared with HFOs synthesized from iron chloride solutions (0.5 mol/L [Cl] and 3.8×10^{-3} M [Au]; and 0.03 mol/L [Cl] and 3.8×10^{-3} [Au]) show XANES spectra which indicate the presence of trivalent gold. At low pH values (5.26 and 5.69), the Au-L_{III} edge XANES spectra are consistent with a mixed O/Cl environment, richer in O than in Cl. At higher pH values (>6), XANES spectra are close to that for crystalline Au_2O_3, indicating the presence of square-planar AuO_4 moieties. The Au-L_{III} edge EXAFS spectra for these samples and their Fourier Transform (FTs) are presented on Figures 12b,c. The results of EXAFS analysis for the first neighbors are presented in Table 4 and Figure 12d. At high pH values (>6), AuO_4 moieties are detected, consistent with previous XANES observations. At low pH values, mixed O/Cl environments are observed (ratio of 3/1), with "standard" Au-O and Au-Cl distances (2.0 and 2.3 Å) and small disorder parameters.

3.3.3. *Second-neighbor Fe around Au(III) adsorbed on HFOs*

In the Au(III)/HFO adsorption samples with the highest Au adsorption densities, there is some evidence in the FTs (see Figs. 10c, 11c, and 12c) for Fe second neighbors at distances of 2.5–3 Å (3.1–3.3 Å when corrected for phase-shifts). These Au-Fe pair contributions are thus located at distances similar to those determined for the Au(III)/goethite adsorption samples. However, the magnitude of these contributions in the Au(III)/HFO adsorption samples is much lower, suggesting larger disorder for these Au-Fe pairs. Because the Au-O environment is similar among goethites and ferrihydrites, the bond valence requirements for the oxygens around Au connecting to Fe must be similar, suggesting that the connectivity between AuO_4 and FeO_6 units must be similar in goethite and in ferrihydrite. RMC methods will help to understand these features (see discussion section).

4. DISCUSSION

4.1. The Local Environment of Au(III) in Aqueous Solutions Versus that of Au(III) Adsorbed on Mineral Surfaces

A summary of the Au(III)-speciation information is shown on Figure 13. The interpretation of the Raman scattering and XANES spectroscopy data for the Au(III)-containing solutions in this study is consistent with previous studies (Peck et al., 1991; Farges et al., 1993; Murphy et al., 1998). For example, we observe that the replacement of Cl ligands around Au by OH ligands starts at pH 4. Murphy and coworkers reported the onset of Cl/O replacement to occur at pH 3.8. However, Peck et al. (1991) reported a higher pH (5.8) for such replacement. These differences are related to the Au/Cl ratio of our solutions,

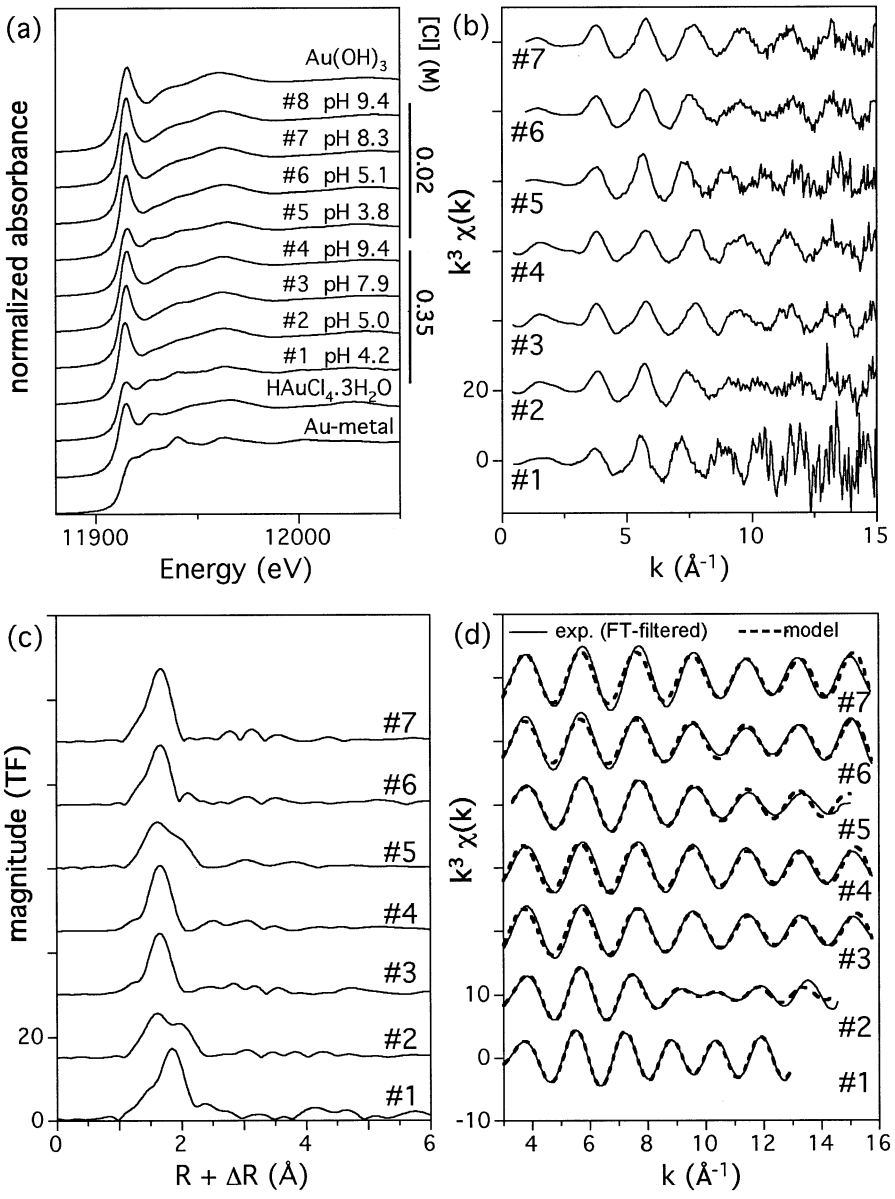

Fig. 10. (a) XANES spectra of gold adsorbed on ferrihydrite from solutions containing 0.35 mol/L [Cl] and 3.0 mM [Au] and 0.02 mol/L [Cl] and 3.0 mM [Au]; (b) k^3-weighted EXAFS spectra for gold adsorbed on ferrihydrite; (c) Fourier Transform of the k^3-weighted EXAFS spectra of gold adsorbed on ferrihydrite; (d) Fits of k^3-weighted EXAFS spectra for gold adsorbed on ferrihydrite.

which were much closer to these reported by Murphy et al. (1998). These results confirm that $AuCl_4$ moieties are present in solution if there is enough Cl to complex Au(III) and if the pH is relatively low (e.g., < 5). With increasing pH, hydroxyl groups tend to progressively replace chloride ions within the square-planar units. In a number of experiments in which gold uptake was not too high, we observed that the speciation of Au(III) in solutions remains unaffected by the adsorption process.

The same trends observed for the coordination environments of Au(III) in solution as a function of Cl/O ratio are also observed for Au(III) adsorbed on the surfaces of HFO, goethite, and boehmite. For example, for Au/Cl ratios < 0.3, a progressive replacement of Au-Cl bonds by Au-O bonds is observed with increasing synthesis pH. However, at any given pH, there are always more Au-O bonds on these surfaces than in the corresponding solutions (before or after uptake). For example, near pH 6.5, Cl-rich moieties are detected in the native solution—a result that contrasts strongly with the subsequent adsorbed moieties, which are dominated by oxygen ligands. This phenomenon was observed for all mineral surface investigated in this study.

4.2. Reverse Monte Carlo Simulations of the EXAFS Spectra

RMC methods were first applied to the analysis of EXAFS spectra of amorphous and crystalline silicon and AgBr (Gur-

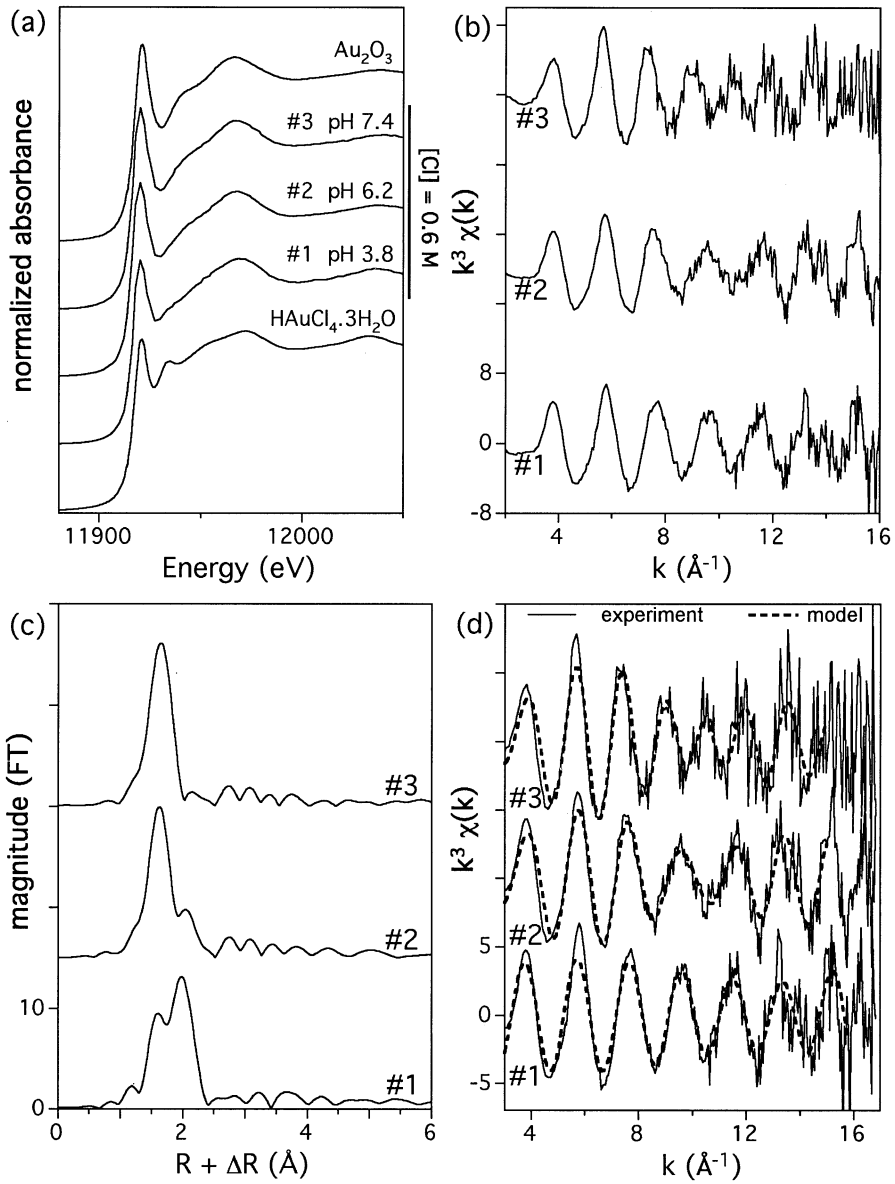

Fig. 11. (a) XANES spectra of gold adsorbed on ferrihydrite from a solution containing 0.6 mol/L [Cl] and 6.0 mM [Au]; (b) k^3-weighted EXAFS spectra for gold adsorbed on ferrihydrite; (c) Fourier Transform of the k^3-weighted EXAFS spectra of gold adsorbed on ferrihydrite; (d) Fits of k^3-weighted EXAFS spectra for gold adsorbed on ferrihydrite.

man and McGreevy, 1990). Such simulations were originally developed by McGreevy and Pusztai (1988) for the analysis of neutron scattering data of liquids. As for any RMC model, the computed solution is not unique and represents a particular simulation of the structure probed (here, the local structure around Au at the goethite/water interface). However, the simulation presented here is an average of 20 different configurations around Au and, therefore, has a higher probability of representing the system probed than simple models based on the fitting of Au-Fe EXAFS contributions. An alternative solution, known by glass scientists for two decades, is to simulate (not to model) a structure, based on a more or less constrained adjustment of the simulation to the experiment. In spite of their intrinsic limitations (only one solution, simplistic metal/oxide interface, etc.), disorder effects can be estimated and compared to the standard EXAFS analysis approach.

In this study, we used the "RMC-XAFS" package (details on the method can be found in Winterer et al., 2002). The starting periodic model was constructed using a double (110) goethite surface (crystal structure information from Gualtieri and Venturelli, 1999) separated by a layer of water. Because protons do not contribute significantly to EXAFS spectra, they were neglected in the model. On both (110) surfaces, twenty iron atoms were replaced by gold atoms (hence in sixfold coordination before the refinement). During each cycle of refinement, all atomic positions were allowed to vary on both the (110) surfaces and in the water layer. Only variations that improved the model quality (based on a χ^2 test) were accepted. After 1000

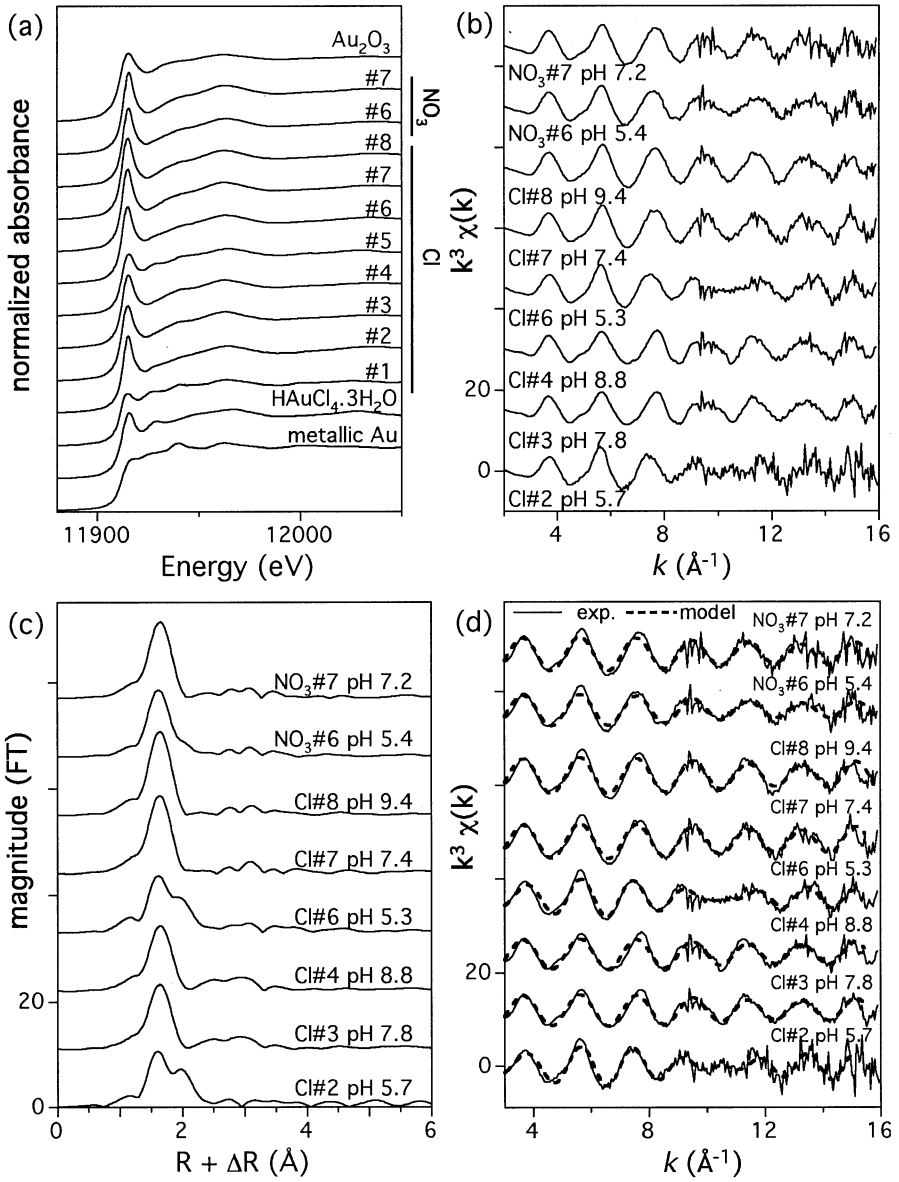

Fig. 12. (a) XANES spectra of gold adsorbed on ferrihydrite (synthesized with iron chloride) from solutions containing 0.5 mol/L [Cl] and 3.8 mM [Au] and 0.03 mol/L [Cl] and 3.8 mM [Au]; (b) k^3-weighted EXAFS spectra for gold adsorbed on ferrihydrite; (c) Fourier Transform of the k^3-weighted EXAFS spectra of gold adsorbed on ferrihydrite; (d) Fits of k^3-weighted EXAFS spectra for gold adsorbed on ferrihydrite.

cycles, the calculated model matches all EXAFS features above 3 Å (Figs. 14a,b). The higher residuals at low energy are attributed to the high-order MS contributions of the XANES that were not included in the model. More details on this rmc model are presented elsewhere (Winterer and Farges, 2004). Figure 14c shows the average partial distribution functions (g(R)) calculated around Au, as well as the gold coordination that one can derive by integration of the g(R). Figure 14d shows atomic-level details for the resulting goethite/water double interface refined using RMC methods. The reverse Monte Carlo analysis of the Au-O pairs is consistent with the EXAFS information derived from classical fitting methods: 4.1 oxygen atoms surrounding, on average, gold, at a distance of 1.94 Å. There are some unrealistically low Au-O distances (near 1.80 Å) created by the RMC model due to the hard sphere restriction imposed using this model (limit set at 1.8 Å around Au). This restriction explains why the modeled Au-O distance is slightly lower than that fit using conventional EXAFS methods (1.99 Å). A second shell of oxygen neighbors is detected near 2.4 Å, and is related to distant oxygens ("water" molecules in the water layer). Iron next-nearest neighbors are distributed around a continuum of Au-Fe distances, ranging from 2.8 to 3.6 Å, with three major contributions centered around 3.0 (N Fe ~ 1 atom), 3.3 (N Fe ~ 0.5 atom), and 3.5 Å (N Fe ~ 1 atom). These average values are close but significantly different from those obtained from classic EXAFS curve-fitting methods (~ 2 Au-Fe contribution near 3.1 and 3.3 Å). Therefore, based on RMC simulations, the adsorbed gold sites on the goethite

Table 3. Synthesis conditions and EXAFS parameters for first neighbors around Auadsorbed on HFO.

Sample	pH[a]	[Au][b] (%)	[Au][c] (mmol/m^2)	Type and number of first neighbors		d(Au-X) (Å)		$\Delta\sigma^2 \times 10^{-3}$ (Å^2)	$\Delta C_3 \times 10^{-4}$ (Å^3)	ΔE_0 (eV)
				0.35 M [Cl] and 3.0 mM [Au]						
HFO #1	4.2	0.554	0.047	O	2.2	2.01		0	0.12	−6.3
				Cl	2.4	2.28		0	0	+6.0
HFO #2	5.0	1.838	0.155	O	3.1	1.99		0	0	−0.9
				Cl	1.1	2.28		0	0.15	+2.0
HFO #3	7.9	3.286	0.276	O	4.2	1.99		−0.6	0	+0.3
HFO #4	9.4	2.948	0.248	O	4.1	1.99		−1.0	0	+0.1
				0.017 M [Cl] and 3.0 mM [Au]						
HFO #5	3.8	3.44	0.289	O	3.2	2.00		0	0	0
				Cl	1.3	2.27		0	0	0
HFO #6	5.1	3.85	0.324	O	3.7	2.00		−1.4	0	+2.2
HFO #7	8.3	3.34	0.281	O	4.3	1.99		−1.3	0	+2.5
HFO #8	9.4	3.38	0.284	O	4.2	1.99		0	0	0
				0.6 M [Cl] and 6.0 mM [Au]						
HFO #1	4.5	1.15	0.097	O	1.9	2.01	2.29	0	0	0
				Cl	2.6			0	0	0
HFO #2	6.2	5.65	0.478	O	3.2	1.98		0	0	0
				Cl	1.0	2.26		0	0	0
HFO #3	7.4	6.48	0.520	O	4.5	1.99		−0.8	0	+1.3
error	0.03	0.03	0.003		0.5	0.02		0.001	0.0001	

[a] pH after equilibration between the solid and the solution.
[b] [Au] concentration in the solid phase in % (*i.e.*, g of Au per 100 g dry weight HFO).
[c] Using a surface area of 600 m^2 g^{-1} as recommended by Davis (1977) and Dzomback and Morel (1990).

surface are distributed over a broad continuum of Au-O-Fe angles. This simulation is in excellent agreement with the wavelet analysis of the EXAFS for Au on goethite in which the Au-Fe pairs appear as a broad contribution (see Fig. 3). This anharmonicity in the site distribution around gold cannot be modeled accurately assuming two sets of Au-Fe distances, which does not provide enough asymmetry to model the medium-range environment around Au. Also, we observed some strong phase-cancellation (ϕc) in the wavelet analysis of the EXAFS contributions for first and next-nearest neighbors (see ϕc in Fig. 3b), which makes the averaged EXAFS signal significantly less informative about of the actual structure of adsorbed Au(III) surface structure (hence this demonstrates the need to use simulations instead of modelizations at this point of the study to determine the range of validation for the EXAFS fits).

Based on this result, we suggest that the conventional EXAFS-derived Au-Fe distances represent a simplification of the Au-Fe bonding simulated by RMC methods. In addition, the EXAFS-derived number of Fe next-nearest neighbors ($\sim$ 2) is an approximation, as it increases continuously with increasing distance to $\sim$3 from the central gold atoms. Finally, Au-Au pairs are detected only above 4.5 Å but second-neighbor Au atoms are too disordered to be detected through this RMC

Table 4. Synthesis conditions and EXAFS data reduction parameters for first neighbors around Au adsorbed on HFO.

Sample	pH[a]	[Au][b] (%)	[Au][c] (mmol/m^2)	Type and number of first neighbors		d(Au-X) (Å)	$\Delta\sigma^2 \times 10^{-3}$ (Å^2)	$\Delta C_3 \times 10^{-4}$ (Å^3)	ΔE_0 (eV)
				0.5 M [Cl] and 3.8 mM [Au]					
HFO Cl_3 2	5.7	1.55	0.131	O	3.2	2.02	0	0	0
				Cl	0.7	2.29	0	0	0
HFO Cl_3 3	7.8	9.89	0.832	O	3.7	1.99	−0.8	0	−0.8
HFO Cl_3 4	8.8	9.33	0.785	O	3.6	1.99	−0.9	0	−0.9
				0.03 M [Cl] and 3.8 mM [Au]					
HFO Cl_3 6	5.3	n.m. (b)	n.m.	O	3.0	2.01	0	0	0
				Cl	0.9	2.29	0	0	0
HFO Cl_3 7	7.4	n.m.	n.m.	O	4.0	1.99	−1.0	0	−0.8
HFO Cl_3 8	9.4	5.9	0.497	O	4.3	1.99	−0.8	0	−0.9
				0.04 M [Cl] and 4.0 mM [Au]					
HFO NO_3 6	5.4	n.m.	n.m.	O	3.9	1.99	0	0	−1.0
HFO NO_3 7	7.2	2.49	0.210	O	4.1	2.00	−0.5	0	−0.8

[a] pH after equilibration between the solid and the solution.
[b] [Au] concentration in the solid phase in % (i.e., g of Au per 100 g dry weight HFO).
[c] Using a surface area of 600 m^2 g^{-1} as recommended by Davis (1977) and Dzomback and Morel (1990).

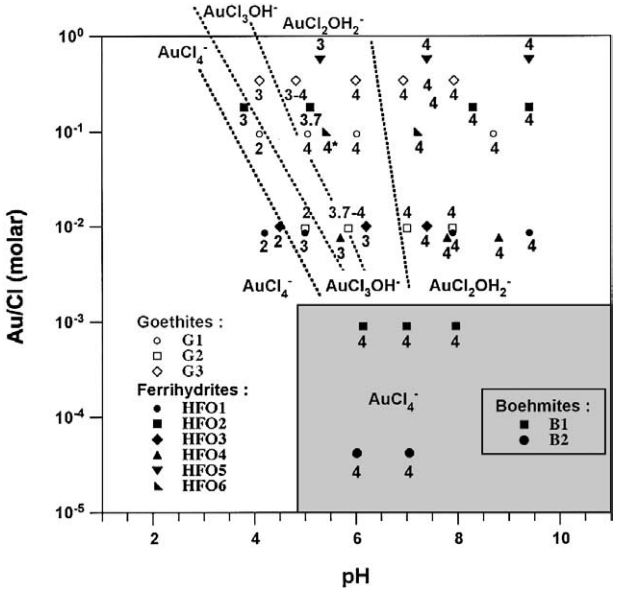

Fig. 13. Summary of the Au(III)-speciation information for the Al/Fe oxy-hydroxydes investigated in that study, showing the fields for $Au(O/OH)_4$, $AuCl(O/OH)_3$ and $AuCl_2(O/OH)_2$ moieties (labeled respectively "4," "3" and "2").

analysis. Consequently, RMC models with lower Au surface coverages would result in similar results, although the statistics (i.e., the number of adsorbed sites for Au) would be too low. Systematic RMC analysis of EXAFS spectra for absorbates will soon be possible when the next generation of computers will provide the CPU time required for these simulations.

4.3. Adsorption Mechanisms of Trivalent Gold

The observed differences in gold speciation at the mineral/water interfaces examined in this study can be related to either a change in gold speciation during uptake, or to preferential absorption of more favorable Au species (O-rich ones) onto the surfaces (as solutions can show a variety of Au species, especially in the pH range 5–9). However, under acidic conditions, Au adsorption is nearly complete. In HFO reacted with a solution containing [Cl] = 0.02 mol/L and [Au] = 3.0×10^{-3} M, for instance, more than 99% of the total Au was adsorbed, leaving an essentially Au-free supernatant, as determined by inductively coupled atomic emission spectroscopy. Under these conditions, there are major differences in gold speciation in aqueous solution vs. the mineral surfaces. The dominant solution species is $AuCl_4^-$ with four Cl^- ligands, whereas adsorbed Au species have only two Cl ligands. This change could occur by adsorption of O-bearing gold complexes in solution as suggested by Machesky et al. (1991), followed by a reequilibration of the solution (imposed by the pH and the Au/Cl molar ratio). This reequilibration of the solution will instantaneously produce a new quantity (even infinitesimal) of O-bearing moeties, with short lifetimes in solution because they will adsorb efficiently onto the surface. At low pH, these Au-OH_n moieties have a rather low concentration (Peck et al., 1991; Murphy et al., 1998), which could explain why the absorption of gold increases with increasing pH as shown by Machesky et al. (1991).

Our spectroscopic information also shows that the adsorption of Au(III) from chloride solutions onto iron/aluminum hydroxides surfaces proceeds via inner-sphere complexation (because of the presence of Al/Fe second neighbors). In addition, changes in the structure of the mineral surface may also play a key role in the speciation of gold. We can compare, for example, the adsorption of gold on HFO synthesized from iron nitrate (in Table 4, HFO NO_3, 6 and 7) with HFO synthesized from iron chloride (in Table 3, HFOCl_3, 6 and 7) but equilibrated under the same solution conditions ([Cl] = 0.03 mol/L and [Au] = 3.8×10^{-3} M (chloride) and [Cl] = 0.04 mol/L and [Au] = 4×10^{-3} M (nitrate). We can expect a larger contribution of Au-Fe pair correlations to the EXAFS spectra of the HFOs synthesized from iron chloride vs. those synthesized from iron nitrate because the former were shown to be slightly more ordered (Bottero et al., 1993). However, at pH 5 and 7, the XAFS spectra for both series of HFOs are similar. More significant "ordering" of the Au-Fe pairs could perhaps be obtained by adsorbing Au(III) onto natural goethite surfaces because its specific area is typically much less than that of HFOs.

In a number of HFO samples where the signal-to-noise ratio is more favorable, we can detect Au-Fe contributions at high R-values (above 2.5 Å), quite similar to those observed in the Au(III)/goethite samples. Therefore, the adsorption mechanism for Au(III) on HFOs may be similar to that for goethite, although the EXAFS data for the Au(III)/HFO adsorption samples cannot be analyzed quantitatively. Au-Al contributions to the EXAFS spectra are more difficult to detect in the case of Au(III)/boehmite adsorption samples because of the significantly lower photoelectron backscattering of Al vs. Fe.

4.4. Bond Valence Constraints on Au(III) Adsorption Modes

Whatever the exact mechanism(s) of Au(III) adsorption on goethites, HFOs, or boehmite, the above observations suggest that oxygen ligands play a key role at the mineral/water interface during the adsorption of gold. Pauling's bond valence considerations (see Pauling, 1929; Brown and Altermatt, 1985; Farges et al., 1991; Manceau and Gates, 1997; Bargar et al., 1997a,b,1998) indicate that monovalent chloride ions are not likely to form a "bridge" between two trivalent (hence, highly-charged) cations (Al/Fe^{3+} and Au^{3+}) when Au(III) adsorbs on Al(III)-Fe(III)-(oxy)hydroxide surfaces. This is because the valence of chloride ions is too low (−1) to accommodate two highly charged cations such as $^{[6]}$Fe(III) and $^{[4]}$Au(III) (these two cations will provide 0.5 and 0.75 valence units, respectively, which exceeds the Pauling bond valence sum of 1 vu required for Cl by Pauling's second rule). The observation of Cl first neighbors around Au in goethite at pH 4 by Heasmann et al. (1998) is, therefore, at variance with our results and, furthermore, cannot be explained in terms of Pauling's bond valence rule. The molecular aspects of Au(III) adsorption on Fe(III)/Al(III)-(oxy)hydroxides is discussed in more detail in Berrodier (2001), including the connectivity of the Fe/Al-O/Cl-Au polyhedra based on the Raman scattering and XAFS spectroscopy information presented above. Part II will also

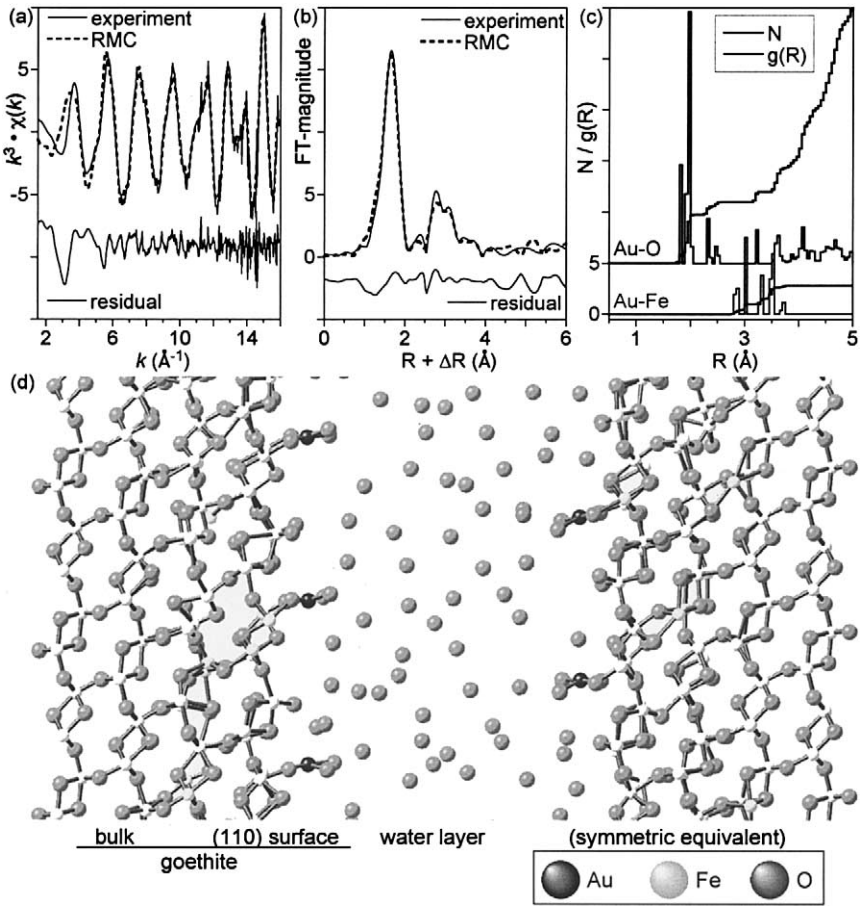

Fig. 14. RMC models results (top three figures); (a) left: in k-space, (b) middle: in R-space; (c) right: coordination number (N) and partial distribution function around Au(III) (g(R)) calculated from the RMC model; bottom figure: zoom on the 3D view of the RMC model, showing the goethite/water interface with Au(III) atoms (in black) adsorbed on the goethite surface and the relaxed water layer (hydrogens were not computed as they do not backscatter x-rays significantly to be detectable in the EXAFS spectrum).

present the results of potentiometric titration experiments that were performed to help constrain the type(s) of Au(III) species present on the mineral surfaces, as XAFS methods are not sensitive to protons and Raman scattering methods cannot be currently used to provide information for Au(III) species on Fe-rich surfaces. This information will be combined and refined using Pauling bond valence models and models of adsorption predicted with the CD-MUSIC model (Hiemstra and Van Riemsdijk, 1996) to develop a molecular-scale view of gold adsorption mechanisms on Fe(III)/Al(III)-(oxy)hydroxides.

5. CONCLUSIONS

Analysis of XANES and EXAFS data collected at the Au-L_{III} edge for crystalline model compounds and Au(III) adsorbed on goethite/HFO is complex and requires special data analysis methods. We have applied several recently developed methods, including spectral deconvolution, principal component analysis, spectral inversion, and wavelet analyses, to evaluate (1) the redox states of Au, (2) X-ray beam-induced Au(III) photo-reduction kinetics, (3) multi-electronic excitations, (4) multiple-scattering features, (5) the number and identity of and distance to first and more distant neighbors around Au, (6) the *k*-range required for deriving statistically robust structural models of the local environment of Au in these types of samples, (7) potential artifacts in the data due to anharmonic effects, and (8) possible destructive interferences that can potentially reduce the information content of EXAFS spectra unless detected. We have shown that for XAFS studies of Au(III) adsorbed on iron/aluminum (oxy)hydroxides, a significant EXAFS *k*-range is required to fit the experimental data (out to k=15 Å^{-1}, at least). The model requires at least three contributions: (1) single-scattering from first neighbors, which can be split into separate O and Cl shells; (2) multiple-scattering arising from these neighbors, which involves at least two contributions, with 3- and 4-leg paths; and (3) a single-scattering contribution involving Fe/Al next-nearest neighbors, which are also often split into at least two significant contributions. Reverse Monte Carlo models of gold adsorption on the (110) surface of goethite suggest the presence of a continuum of Au-O-Fe angles, resulting in a highly asymmetric $g_{Au\text{-}Fe}(R)$ between 2.8 and 3.6 Å. Classical EXAFS models are now believed to report mostly the statistical centroids for each cumulant in that asymmetry.

Based on these constraints, EXAFS spectroscopic studies show that Au(III) adsorbs from chloride solutions on ferrihydrite, goethite, and boehmite surfaces dominantly as inner-sphere, square-planar complexes, all with relatively low degrees of distortion. Gold adsorbed on goethite and ferrihydrite is present dominantly as $Au(III)O_4$ complexes at pH $\geq$ 6, and as $Au(III)(O,Cl)_4$ complexes at pH $<$ 6, with the number of Cl ligands generally increasing as pH decreases and [Cl] increases. Gold adsorbed on boehmite at pH 6–8 is present as $Au(III)O_4$ surface complexes. Thus, the redox state of Au remains unchanged during adsorption on these phases. The weak contribution arising from second-neighbor Fe around Au(III) adsorbed on HFOs did not allow us to quantitatively model the EXAFS spectra of these samples. However, by comparing the Au(III)/HFO adsorption sample data with those for the Au(III)/goethite and Au(III)/boehmite adsorption samples, a consistent model of Au(III) adsorption on Fe(III)- and Al(III)-(oxy)hydroxides can be developed. The structural models integrating these data and potentiometric titration data are to be detailed in Berrodier (2001) and in Part II of that series (in preparation). This next paper will show that, based on spectroscopic and titrations experiments together with bond valence considerations that $Au(III)(O,Cl)_4$ units are bonded as inner-sphere, bidentate binuclear and monodentate (corner-shared) complexes with $Fe(O,OH)_6$ and $Al(O,OH)_6$ octahedra on the Fe(III)-(oxy)hydroxide and boehmite surfaces, respectively, with Au-O-Al/Fe angles of 100–110°. The overall good agreement between spectroscopic and thermodynamic models confirms the paucity of the structural model based on spectroscopy, RMC and bond valence theory. Then, from the use of the CD-MUSIC package, the various Au-sorbed species (such as $Fe(OH)_2AuCl_2$, $Fe(OH)_2AuClOH$, $Fe(OH)_2AuOH_2$, $(Fe_3(OH))_3Au(OH)_2$, etc.) can be identified as a function of pH. However, some minor discrepancies (especially at pH $>$ 8) are attributed to neglecting of potentially active sites on the surface of goethite, such as these observed on the (021) face.

Acknowledgments—We thank the staffs of SSRL (Stanford, California) and LURE (Orsay, France), particularly John R. Bargar (SSRL) and Robert Cortes and Isabelle Ascone (both at LURE), for their help with data collection. Guillaume Morin (CNRS at the Laboratoire de Minéralogie-Cristallographie, Université de Paris 6 and 7) kindly donated the boehmite samples. We also thank Mohammed Talbi (CGI-ENSMP at the Université de Marne la Vallée, France), Rossana Combes (CESAM-Université de Marne la Vallée, France), Daniel Neuville (CNRS-IPGP, Paris), and Christophe Lefebvre (CEA, Fontenay aux Roses) for their help in collecting XRD, ESEM, Raman scattering, and specific surface area (BET) information. This work is a part of the Ph.D. work of Ingrid Berrodier, defended February 2001 at the Centre de Géologie de l'Ingénieur of the Ecole Nationale Supérieure des Mines de Paris. Critical reviews from François Martin (University of Toulouse III-Paul Sabatier), Philippe Freyssinet (BRGM, Orléans, France), Alain Manceau (CNRS, Grenoble, France), and Robert Cortes (LURE, Orsay, France) greatly improved the manuscript, as well as three anonymous reviewers. Jacques Schott is thanked as well for many constructive comments and his luminous idea to merge two already indigestible manuscripts into one even bigger. This research was supported by CNRS (Farges) and by NSF Grants INT-9726528 (Brown) and CHE-0089215 (Brown). The Stanford Synchrotron Radiation Laboratory is supported by the DOE, Office of Basic Energy Sciences, and NIH, Biotechnology Resource Program, Division of Research Resources.

Associate editor: J. Schott

REFERENCES

Ankudinov A. L., Ravel B., Rehr J. J., and Conradson S. D. (1998) Real-space multiple scattering calculation and interpretation of x-ray absorption near-edge structure. *Phys. Rev. B* **58,** 7565–7576.

Bargar J. R., Brown G. E., Jr., and Parks G. A. (1997a) Surface complexation of Pb(II) at oxides water interfaces. I. XAFS and bond valence determination of mononuclear and polynuclear Pb(II) sorption products on aluminum oxides. *Geochim. Cosmochim. Acta* **61,** 2617–2637.

Bargar J. R., Brown G. E., Jr., and Parks G. A. (1997b) Surface complexation of Pb(II) at oxide/water interfaces. II. XAFS and bond valence determination of mononuclear Pb (II) sorption products and surface functional groups on iron oxides. *Geochim. Cosmochim. Acta* **61,** 2639–2652.

Bargar J. R., Brown G. E., Jr., and Parks G. A. (1998) Surface complexation of Pb(II) at oxide/water interfaces. III. XAFS and bond valence determination Pb(II) and Pb(II)-chloro adsorption complexes on goethite and alumina. *Geochim. Cosmochim. Acta* **62,** 193–207.

Bassi I. W., Lytle F. W., and Parravano G. (1976) Chemical reactivity of supported gold III. Atomic binding and coordination of gold from X-ray absorption fine structure spectroscopy. *J. Catalysis* **42,** 139–147.

Benedetti M. F. and Boulegue J. (1990) Mechanisms of gold transfer and deposition in a supergene environment. *Geochim. Cosmochim. Acta* **55,** 1539–1547.

Benfield R. E., Filipponi A., Bowron D. T., Newport R. J., and Gurman S. J. (1994) X ray absorption study of gold compounds: EXAFS refinements and double excitation background. *J. Phys. Cond. Matter* **6,** 8429–8448.

Berrodier I. (2001) Etude des mécanismes d'adsorption de l'or(III) sur des surfaces d'oxyhydroxydes de fer et d'aluminium. Ph.D. thesis, Ecole Nationale Supérieure des Mines de Paris.

Berrodier I., Farges F., Benedetti M. and Brown G.E. Jr.(1998) Adsorption of Au on iron oxy-hydroxides using Au-L_3 edge XAFS spectroscopy. In: *XAFS X Book of Abstracts*, p. 157. Munskgaard International Booksellers and Publishers for the International Union Crystallography.

Berrodier I., Farges F., Benedetti M., and Brown G. E., Jr.. (1999) Adsorption of Au on ferrihydrites using Au-LIII edge XAFS spectroscopy. *J. Synchrotron Rad.* **S6,** 651–652.

Bottero J. Y., Arnaud M., Villieras F., Michot L., De Donato P., and François M. (1993) Surface and textural heterogeneity of fresh hydrous ferric oxides in water and in the dry state. *J. Colloid Interface Sci.* **159,** 45–52.

Bowell R. J., Foster R. P., and Gize P. (1993a) The mobility of gold in tropical rain forest soils. *Econ. Geol.* **88,** 999–1016.

Bowell R. J., Gize P., and Foster R. P. (1993b) The role of fluvic acid in the supergene migration of gold in tropical rain forest soils. *Geochim. Cosmochim. Acta* **57,** 4179–4.

Brown G. E., Jr.. (1990) Spectroscopic studies of chemisorption reaction mechanisms at oxide/water interfaces. *Rev. Mineral.* **23,** 309–363.

Brown I. D. and Altermatt D. (1985) Bond valence parameters obtained from a systematic analysis of the inorganic crystal structure database. *Acta Crystallogr.* **B 41,** 244.

Brown G. E., Jr., Henrich V. E., Casey W. H., Clark D. L., Eggleston C., Felmy A., Goodman D. W., Grätzel M., Maciel G., McCarthy M. I., Nealson K. H., Sverjensky D. A., Toney M. F., and Zachara J. M. (1999) Metal oxide surfaces and their interactions with aqueous solutions and microbial organisms. *Chem. Rev.* **99,** 77–174.

Brown G. E., Jr. and Parks G. A. (2001) Sorption of trace elements from aqueous media: Modern perspectives from spectroscopic studies and comments on adsorption in the marine environment. *Int. Geol. Rev.* **43,** 963–1073.

Butt C.R.M. (1988) The dispersion of gold in the weathered zone, Yildarn Block, Western Australia. In: *Proceedings of the Australian Geology Society Meeting*, Perth, October 1987, pp. 27–53. Australian Geology Society.

Castet S., Dandurand J. L., Schott J., and Gout R. (1993) Boehmite solubility and aqueous aluminum speciation in hydrothermal solu-

tions (90–350°C): Experimental study and modeling. *Geochim. Cosmochim. Acta* **57,** 4869–4884.
Colin F., Lecomte P., and Boulange B. (1989) Dissolution features of gold particles in laterite profile from Dondo Mobi, Gabon. *Geoderma* **45,** 241–250.
Colin F. and Vieillard P. (1991) Behavior of gold in lateritic equatorial environment: Weathering and surface dispersion of residual gold particles at Dondo Mobi, Gabon. *Appl. Geochem.* **6,** 279–285.
Colin F., Vieillard P., and Ambrosi J. P. (1993) Quantitative approach to physical and chemical gold mobility in equatorial rainforest lateritic environment. *Earth Planet. Sci. Lett.* **114,** 269–285.
Combes J. M., Manceau A., Calas G., and Bottero J. Y. (1989) Formation of ferric oxides from aqueous solutions: A polyhedral approach by x-ray absorption spectroscopy. I. Hydrolysis and formation of ferric gels. *Geochim. Comsochim. Acta* **53,** 583–594.
Crozier E. D., Rehr J. J., and Ingalls R. (1988) Amorphous and liquid systems. In: *X-ray Absorption: Principles, Applications, Techniques of EXAFS, SEXAFS and XANES* (eds. D.C. Koningsberger and R. Prins), pp. 373–442. Wiley.
Davis J.A. (1977) Adsorption of trace metals and complexing ligands at the oxide/water interface. Ph.D. thesis, Stanford University.
Drits V. A., Sakharov B. A., Salyn A. L., and Manceau A. (1993) Structural model for ferrihydrite. *Clay Minerals* **28,** 185–207.
Dzomback D. A. and Morel F. M. M. (1990) Surface Complexation Modeling: Hydrous Ferric Oxide. Wiley.
Farges F., Ponader C. W., and Brown G. E., Jr.. (1991) Local environment around incompatible elements in silicate glass/melt systems. I: Zr at trace levels. *Geochim. Cosmochim. Acta* **55,** 1563–1574.
Farges F., Sharps J. A., and Brown G. E., Jr.. (1993) Local environment around gold(III) in aqueous chloride solutions: An EXAFS spectroscopy study. *Geochim. Cosmochim. Acta* **57,** 1243–1252.
Farges F. and Brown G. E., Jr.. (1996) An empirical model for the anharmonic analysis of high-temperature XAFS spectra of oxide compounds with applications to the coordination environment of Ni in Ni-olivine and Ni-Na-disilicate glass and melt. *Chem. Geol.* **127,** 253–268.
Farges F., Brown G. E., Jr., and Rehr J. J. (1996) Coordination chemistry of Ti(IV) in silicate glasses and melts. I. XAFS study of Ti coordination in oxide model compounds. *Geochim. Cosmochim. Acta* **60,** 3023–3038.
Farges F., Neuville D. R., and Brown G. E., Jr.. (1999) Coordination chemistry of trace levels of Pt(IV) in silicate glasses: An x-ray absorption fine structure (XAFS) spectroscopy study. *Am. Mineral.* **84,** 1562–1568.
Fedoseyeva V. I. and Strel'tsova O. A. (1987) The adsorption interaction of aluminum oxide with the Au(I) thiosulfate complex. *Geochem. Intl.* **24,** 117–119.
Fedoseyeva V. I. and Zvonareva G. V. (1988) Gold(III) hydroxochloride-complex adsorption on aluminum oxide. *Geochem. Intl.* **25,** 115–119.
Filipponi A. (2000) Deconvolution of the lifetime broadening from X-ray absorption spectra of atomic and molecular species. *J. Phys. B* **33,** 2835–2846.
Filipponi A., Dicicco A., Tyson T. A., and Natoli C. R. (1991) Ab initio modeling of x-ray absorption spectra. *Sol. State Comm.* **78,** 265–268.
Fressinet P. (1991) Géochimie et minéralogie des latérites du sud Mali: Evolution du paysage et prospection géochimique de l'or. Ph.D. thesis, BRGM 203.
Gréffié C., Benedetti M. F., Parron C., and Amouric M. (1996) Gold and iron oxide associations under supergene conditions: An experimental approach. *Geochim. Cosmochim. Acta* **60,** 1531–1542.
Grimm B. and Friedrich G. (1990) Weathering effects on supergene gold in soils of a semiarid environment, Gentio Do Ouro, Brazil. *Chem. Geol.* **84,** 70–73.
Gualtieri A. and Venturelli P. (1999) In situ study of the goethite-hematite phase transformation by real time synchrotron powder diffraction. *Am. Mineral.* **84,** 895–904.
Gurman S. J. and McGreevy R. M. (1990) Reverse Monte Carlo simulation for the analysis of EXAFS data. *J. Phys. Cond. Matter.* **2,** 9463–9474.
Heasmann D. M., Sherman D. M., and Ragnarsdottir K. V. (1998) An EXAFS study of the adsorption of Au^{3+} from aqueous solutions to goethite. *Mineral. Mag.* **62A,** 589–590.
Hiemstra T. and Van Riemsdijk W. (1996) A surface structural approach to ion adsorption: The charge distribution (CD) model. *J. Colloid Interface Sci.* **179,** 488–508.
Hiemstra T., Van Riemsdijk W., and Bolt G. H. (1989a) Multisite proton adsorption modeling at the solid/solution interface of (hydr)oxides: A new approach. *J. Colloid Interface Sci.* **133,** 91–104.
Hiemstra T., De Witt J. C. M., and Van Riemsdijk W. (1989b) Multisite proton adsorption modeling at the solid/solution interface of (hydr)oxides: A new approach II. Application to various important (hydr)oxides. *J. Colloid Interface Sci.* **133,** 105–117.
Hyland M. M. and Bancroft G. M. (1989) An XPS study of gold deposition at low temperatures on sulfide minerals: Reducing agents. *Geochim. Cosmochim. Acta* **53,** 367–372.
Jean G. E. and Bancroft G. M. (1985) An XPS and SEM study of gold deposition at low temperature on sulfide mineral surfaces: Concentration of gold by adsorption/desorption. *Geochim. Cosmochim. Acta* **49,** 979–987.
Johnson B. B. (1990) Effects of pH, temperature and concnetration on the adsorption of cadmium on goethite. *Environ. Sci. Technol.* **24,** 112–118.
Jones P. G., Rumpel H., Schwarzmann E., and Sheldrick G. (1979) Gold(III) oxide. *Acta Cristallogr.* **B35,** 1435–1437.
Karasyova O. N., Ivanova L. I., Lakshtanov L. Z., Lövgren L., and Sjöberg S. (1998) Complexation of gold(III)-chloride at the surface of hematite. *Aquat. Geochem.* **4,** 215–231.
Klementiev K.V. (2000) VIPER for Windows. Freeware. Available at: http://www.desy.de/~klmn/viper.html.
Krause M. O. and Oliver J. H. (1979) Natural widths of atomic K and L levels, K alpha X-ray lines and several KLL auger lines. *J. Phys. Chem. Ref. Data* **8,** 329–338.
Lytle F. W., Wei P. S. P., Greegor R. B., Via G. H., and Sinfelt J. H. (1979) Effect of chemical environment on magnitude of x-ray absorption resonance at LIII edges. Studies on metallic elements, compounds, and catalysts. *J. Chem. Phys.* **70,** 4849–4855.
Machairas G. (1963) Etude des phénomènes de migration chimique de l'or: Cas de la Guyane Francaise et d'Ity en Cote d'Ivoire. *Bull. Soc. Fr. Minéral. Cristallogr.* **86,** 78–80.
Machesky M. L., Andrade W. O., and Rose A. W. (1991) Adsorption of gold(III)-chloride and gold(I)-thiosulfate anions by goethite. *Geochim. Cosmochim. Acta* **55,** 769–776.
Machesky M. L., Andrade W. O., and Rose A. W. (1992) Interactions of gold(III) chloride and elemental gold with peat-derived humic substances. *Chem. Geol.* **102,** 53–71.
Manceau A. and Drits V. A. (1993) Local structure of ferrihydrite and feroxyhite by EXAFS spectroscopy. *Clay Minerals* **28,** 165–184.
Manceau A. and Gates W. P. (1997) Surface structural model for ferrihydrite. *Clays Clay Minerals* **45,** 448–460.
Mann A. W. (1984) Mobility of gold and silver in lateritic weathering profiles: some observations from Western Australia. *Econ. Geol.* **79,** 38–48.
McGreevy R. L. and Pusztai L. (1988) Reverse Monte Carlo simulation: A new technique for the determination of disordered structures. *Mol. Simul.* **1,** 359–367.
McInnes B. I. A., Dunn C., Cameron E. M., and Kameko L. (1996) Biogeochemical exploration for gold in tropical rain forest regions of Papua New Guinea. *J. Geochem. Explor.* **57,** 227–243.
Michel D. (1987) Concentration of gold in situ laterites from Mato Grosso. *Mineral. Dep.* **22,** 185–189.
Mitsyuk B. M., Mironov A. G., Plyusnin A. M., and Belomestrova N. V. (1991) Gold uptake by silica from dilute chloride, thiosulfate and ammoniacal solutions. *Geochem. Intl.* **28,** 852–859.
Muñoz M., Argoul P., and Farges F. (2003) Continuous Cauchy wavelet transform analysis of EXAFS spectra: A qualitative approach. *Am. Mineral.* **88,** 694–700.
Murphy P. J. and Lagrange M. S. (1998) Raman spectroscopy of gold chloro-hydroxy speciation in fluids at ambient temperature and pressure: A reevaluation of the effects of pH and chloride. *Geochim. Cosmochim. Acta* **62,** 3515–3526.
Mycroft J. R., Bancroft G. M., Mc Intyre N. S., and Lorimer J. W. (1995) Spontaneous deposition of gold on pyrite from solutions containing Au(III) and Au(I)chlorides. Part I: A surface study. *Geochim. Cosmochim. Acta* **49,** 979–987.

Nechayev YE.A. (1984) The effects of solution composition on the adsorption of gold(III) complexes on hematite. *Geochem. Intl.* **21,** 87–93.

Nechayev YE.A. and Nickolenko N. V. (1986) Adsorption of gold(III) chloride complexes on alumina, silica and kaolin. *Geochem. Intl.* **23,** 32–37.

Pauling L. (1929) The principles determining the structure of complex ionic crystals. *J. Am. Chem. Soc.* **51,** 1010–1026.

Peck J. A., Tait C. D., Swanson B. I., and Brown G. E., Jr.. (1991) Speciation of aqueous gold(III) chlorides from ultraviolet/visible absorption and Raman/resonance Raman spectroscopies. *Geochim. Cosmochim. Acta* **55,** 671–676.

Ralle M. and Jansen M. (1993) Synthesis and crystal structure determination of $LaAuO_3$. *J. Sol. State Chem.* **105,** 378–384.

Rehr J. J., Albers R. C., Natoli C. R., and Stern E. A. (1986) New high energy approximation for x-ray-absorption near edge structure. *Phys. Rev. B* **69,** 4350–4353.

Rehr J. J., Albers R. C., and Zabinski S. I. (1992) High order multiple scattering calculations of x-ray-absorption fine structure. *Phys. Rev. Lett.* **69,** 3397–4000.

Reichertz P. and Yost W. (1946) The crystal structure of boehmite. *J. Chem. Phys.* **14,** 495–501.

Sanfo Z., Colin F., Delaune M., Boulange B., Parisor J. C., Bradley R., and Bratt J. (1993) Gold: A useful tracer in subsahelian laterites. *Chem. Geol.* **107,** 323–326.

Schoonen M. A. A., Fisher N. S., and Wente M. (1992) Gold sorption onto pyrite and goethite: A radiotracer study. *Geochim. Cosmochim. Acta* **56,** 1801–1814.

Seward T. M. (1984) The transport and deposition of gold in hydrothermal systems. In: *Gold '82: The Geology, Geochemistry and Genesis of Gold Deposits* (ed. R. P. Foster), pp. 165–182. Balkema.

Solera J. A., Garcia J., and Proietti M. G. (1995) Multielectron excitations at the L edges in rare-earth ionic aqueous solutions. *Phys. Rev. B* **51,** 2678–2686.

Sposito G. (1984) The Surface Chemistry of Soils. Oxford University Press.

Szytula A., Burewicz A., Dimitrijewic Z., Krasnicki S., Rzany H., Todorovic J., Wanic A., and Wolski W. (1968) Neutron diffraction studies of α-FeOOH. *Phys. Stat. Solidi* **26,** 429–434.

Theobald F. and Omrani H. (1980) Structure du tétrachloroaurate(III) de potassium dihydraté. *Acta Cristallogr.* **B36,** 2932–2935.

Tossell J. A. (1996) The speciation of gold in aqueous solution: A theoretical study. *Geochim. Cosmochim. Acta* **60,** 17–29.

Von Hoppe W. (1941) Über die kristallostruktur von α-AlOOH (Diaspor) und α-FeOOH (nadeleisenerz). *Zeit. Kristallogr.* **103,** 73–89.

Venema P., Hiemstra T., and Van Riemsdijk W. (1996) Comparison of different site binding models for cations sorption: Description of pH dependency, salt dependency and cation-proton exchange. *J. Coll. Interf. Sci.* **181,** 45–59.

Watkins J. W., Elder R. C., Greene B., and Darnell D. W. (1987) Determination of gold binding in algal biomass using EXAFS and XANES spectroscopies. *Inorg. Chem.* **26,** 1147–1151.

Waychunas G. A., Fuller C. C., Rea B. A., and Davis J. A. (1996) Wide angle X-ray scattering (WAXS) study of "two-line" ferrihydrite structure: Effect of arsenate sorption and counterion variation and comparison with EXAFS results. *Geochim. Cosmochim. Acta* **60,** 1765–1781.

Webster J. G. and Mann A. W. (1984) The influence of climate, geomorphology and primary geology on the supergene migration of gold and silver. *J. Geochem. Explor.* **22,** 21–42.

Wilson A. F. (1984) Origin of quartz free gold nuggets and supergene gold found in laterites and soils: A review and some new observations. *Australian J. Earth Sci.* **31,** 303–316.

Widler A. M. and Seward T. M. (2002) The adsorption of gold(I) hydrosulphide complexes by iron sulphide surfaces. *Geochim. Cosmochim. Acta* **66,** 383–402.

Winterer M. (1996) The XAFS package. In: *Proceedings of the 9th International Conference on X-ray Absorption Fine Structure* (XAFS VI, Grenoble), *J. Phys. IV, Colloq.*, 7-C2, 243–244.

Winterer M., Delaplane B., and McGreevy R. (2002) X-ray diffraction, neutron scattering and EXAFS spectroscopy of monoclinic zirconia: Analysis by Rietveld refinement and reverse Monte Carlo simulations. *J. Appl. Crystallogr.* **35,** 434–442.

Winterer M., Farges F. (2004) Reverse Monte Carlo simulations of EXAFS spectra: Application to the sorption of gold on iron oxyhydroxides. *Phys. Script.*, in press.

Zeegers H. (1987) Remaniements de surface et prospection géochimique de l'or. *Chronique Rech. Min.* **488,** 55–61.